Establishing a pipeline for structural image processing of the chimpanzee brain and application to structural covariance estimation by unsupervised machine learning

By Sam Vickery (2515263)

Translational Neuroscience Master Thesis

Heinrich-Heine Universität Düsseldorf

October 2018

Eidesstattliche Versicherung / Affirmation in lieu of oath

Ich versichere, dass ich die vorliegende Masterarbeit selbständig verfasst und ohne Benutzung anderer als der angegebenen Hilfsmittel angefertigt, nur die angegebenen Quellen benutzt habe. Ich habe die Stellen gekennzeichnet, die ich wörtlich oder inhaltlich den benutzen Quellen entnommen habe. Die Arbeit hat in gleicher oder ähnlicher Form noch keiner anderen Prüfungsbehörde vorgelegen.

I hereby declare that I have authored the present Master thesis independently and without making use of any means other than those indicated, only using the sources indicated. I marked the passages which I have taken literally or with regards to content from the sources used. The work has not been submitted in the same or similar form to any other examination authority.

I hereby confirm that the printed version of this thesis is identical to the digital version handed in to the examination authority.

(Ort, Datum, Unterschrift des Kandidaten/der Kandidatin /
Place, Date, Signature Candidate)

Meerbusch, 8.10.18,

Table of Contents

List of Abbreviations

AMAP - Adaptive Maximum A Posterior

CAT – Computational Anatomical Toolbox

CSF - Cerebrospinal fluid

DARTEL - Diffeomorphic anatomical registration through exponentiated lie algebra

DICOM - Digital Imaging and Communications in Medicine

FWE - Family Wise Error

FWHM - full width half maximum

GM - Gray matter

GMV - Grey matter volume

ICA - Independent component analysis

IQR - Image Quality rating

LAS - Local adaptive segmentation

LDDMM - large deformation diffeomorphic metric mapping

MRI - Magnetic resonance image

NIfTI - Neuroimaging Informatics Technology Initiative

NNSVD - non-negative double singular value decomposition

NNMF - Non-negative matrix factorization

OPNMF - Orthonormal Projective Non-Negative Matrix Factorization

PCA - Principle component analysis

QC - Quality control

RBM - Region Based Morphometry

ROI - Region of Interest

SANLM - Spatial Adaptive Non-Local-Means

SPM - Statistical Parametric Mapping

TFCE - Threshold-Free Cluster enhancement

TPM -Tissue probability map

TIV - Total intracranial volume

UTMDACC - The University of Texas M.D Anderson Cancer Center

VBM - Voxel Based Morphometry

WM - White matter

WMH - White Matter Hyper-intensities

XML - Extensible Markup Language

YNPRC - Yerkes National Primate Research Center

Abstract

Chimpanzees along with bonobos are the closest extant primate to humans, but human brains are significantly larger with increased gyrification especially when accounting for size. Due to this difference a chimpanzee specific spatial normalization template is needed for accurate image registration when conducting group analysis such as voxel- (VBM) or region-based morphometry (RBM). Therefore, the aim is to provide an outline and show practical application of chimpanzee specific templates and manual macroanatomical annotations created for the Computation Anatomy Toolbox (CAT). Practical application is demonstrated by analyzing the effect aging has on grey matter volume and uncovering structurally co-varying grey matter regions using an unsupervised learning algorithm, non-negative matrix factorization (NNMF).Structural T1-weighted MRI scans of 219 (M = 27.04, SD = 6.74) captive chimpanzees were used in this study (www.chimpanzeebrain.org). The images were processed with CAT using the "greater_apes" setting. This enabled the creation of a greater ape specific tissue probability map (TPM) and DARTEL/Shooting templates which could be used for initial segmentation and spatial registration. This was then able to create chimpanzee specific DARTEL/Shooting templates which could be average to produce a chimpanzee TPM. Afterwards, CAT preprocessing was repeated with the adapted TPM, and DARTEL/Shooting templates producing spatial normalized T1 data maps. The T1 maps were averaged and used to create a macro anatomical atlas with segmentation of the major structures using the Slicer software package Manual quality control (QC) was conducted on the processed images, by consulting the CAT image quality rankings to ensure only the best images would be used for further analysis .The results indicate a significant decline in GMV in response to aging in chimpanzee in particular located in the temporal and frontal cortices which corresponds with previous research in humans and chimpanzees. The initial NNMF results are promising. They showed using relatively low rank component solutions, one can extract solid components that align with some anatomical structures in particular the prefrontal cortex. Therefore, the reliability of processed images could be successfully demonstrated and NNMF could be shown to extract anatomical meaningful structurally co-

varying regions which could be used in future research to understanding primate brain organization and interspecies comparison.

Introduction

Chimpanzees

Chimpanzees along with bonobos are the closest extant relative to humans and therefore, offer a unique opportunity as an animal model to understand human evolution. There is significantly less data on bonobos compared to chimpanzees due to their low numbers in the wild and in captivity. Therefore, investigation of chimpanzees represents a possibility for more robust research. The DNA sequence compared between chimpanzees and humans genome is almost 99% identical (1). Along with the genome, the human and chimpanzee brains are very similar in terms of organization and morphology (fig. 1). The chimpanzee brain has the highest amount of gyrification among the non-human primates (2). Hemispheric asymmetries in cortical thickness which is found in humans can also be seen in chimpanzees (3). Behaviorally chimpanzees are the most advanced of the non-human primates, with their use of tools and complex social environments (4). The brain of a chimpanzee is three times smaller than a humans, but it is not just a smaller replica. This size difference comes along with disproportionately more gyrification (5) and larger parietal(6), and frontal lobe in particular the pre-frontal cortex (7) within the human brain. To understand these similarities and differences one can utilize the techniques of brain morphometry.

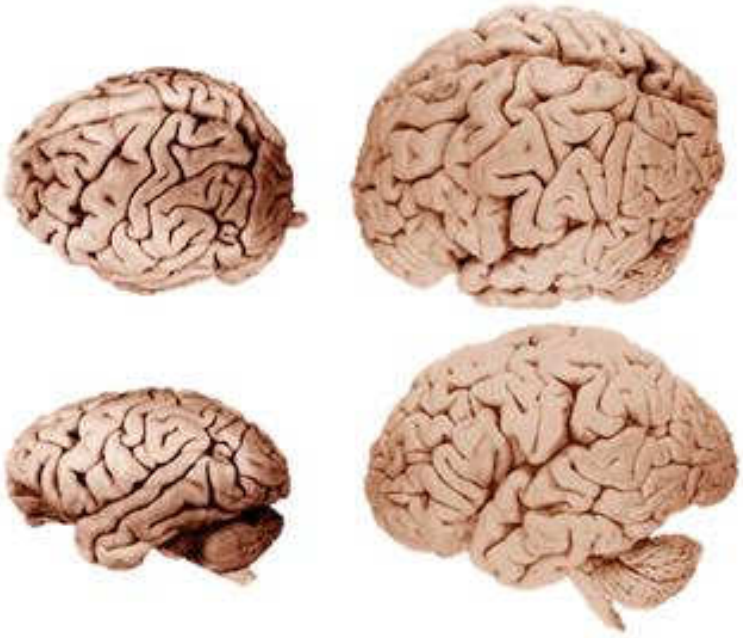

Figure 1. Photographs of the whole brain from a chimpanzee (left) and a human (right). Top are the dorsal-lateral view of the brain and bottom is the lateral view of the brain. Photographs are taken by the University of Wisconsin-Madison Brain Collection (http://neurosciencelibrary.org). Images are not exactly to scale.

Quantifying Brain Morphometry

Brain morphometry is the endeavor to study the size and shape of the brain as a whole and its contained structures. This type of research has been made accessible because of improved computing power and MRI quality. Morphometric changes within the brain can be found in both physiological and pathophysiological states. There are a wealth of examples where these changes have been shown, for instance in brain atrophy during aging (8), localized grey matter volume (GMV) increase in motor skill learning (9), and hippocampal atrophy in Alzheimer's disease (10). With this ability to better understand the healthy and unhealthy brain there is an abundance of research using this modality in the neuroimaging field.

Two of the more popular brain morphometry techniques are voxel-based morphometry (VBM) and region-based morphometry (RBM). Using RBM, the volume of WM and/or GM of a predefined region is extracted and used for statistical analyses. Whereas, VBM is a whole brain voxel-wise analysis. In order to conduct these types of analyses the images must be

preprocessed. This involves spatial registration, segmentation, and in the case of VBM modulation spatial smoothing.

Spatial registration is where the individual brains are linearly and on-linearly registered to a template brain so they can be in the same reference space to enable relative comparisons. Linear registration is when the brain image moves as a whole to align with the template (11), whereas using non-linear registration, local areas deform independent of each other to fit the template (12). Therefore, to conduct pre-processing effectively the template should be as close to the sample being analyzed as possible (13). The process of non-linear pre-processing creates something called a deformation field. The deformation field is a map that indicates how each voxel of the individual brain has been morphed to fit the template. The deformation field is kept for later modulation in VBM (13).

Segmentation is the creation of segment maps of the three main tissue types within the brain, grey matter (GM), white matter (WM), and cerebrospinal fluid (CSF). The tissue segments are determined by the image intensity as well as using tissue probability maps (TPM). The TPMs represent the prior probability that a particular tissue type will be found at a location within the image (14). Modulation is a process, by which voxel intensities are multiplied by the local values of the deformation field from normalization to enable quantification of inter-subject differences. For example, if an area had to shrink by a factor of two then after modulation the intensity would be doubled. Now changes in intensity represent volume relative to the template.

Finally smoothing is conducted to remove remaining inter-individual variance in anatomy for better comparison. Smoothing involves convolving each voxel with an isotropic Gaussian kernel with a predetermined full width at half maximum (FWHM). This insures that each voxel represents a weighted average of its surrounding voxels (15).

Brain Parcellation

Parcellating the brain has been an endeavor of neuroscientist that has spanned the centuries. The intrigue and difficulty in the investigation of the brain is due to its complex topographical organization. A similar topographical organization is shared by all vertebrates.

The brain is organized into distinct areas that share a particular structure and/or function, but these areas are not static. They can vary between people and change due to injury, neuroplasticity, and pathology.

A parcellation can be taken from different scales within the brain and by assessing different aspects of the brains structure and function. There are two major scales of parcellation, microanatomy and macroanatomy. Microanatomy parcellation defines areas based on the morphology and distribution of neurons of the cortex or by looking at neurotransmitter receptor density. This can be seen as the gold standard because the density and distribution of different neuron types within the various layers of the cortex gives a precise definition of a particular area (16, 17). Regions that share the same microanatomical organization usually also share brain function. Microanatomy parcellation requires microscopic analysis of histological sections which is very time consuming and requires post mortem brains. Macroanatomy refers to gross anatomical structures that can be seen without the help of a microscope. Macroanatomy refers to the aspects of the brain that can be extracted using an MRI. This scale has the advantage of large sample sizes, which can both map and better compensate for the interindividual differences. GMV or cortical thickness can be used to parcellate the brain into regions based on their structural covariance.

Structural Covariance

There are large variation in cerebral cortex morphology between individuals across the population. But this is not random, as inter-individual differences of regional brain structures co-vary with inter-individual differences of other regions, in a process known as structural covariance (18). This shared variation can be assessed using VBM to uncover the regional co-varying GMV networks (19). A problem with these structural co-variance networks is their interpretability. It is not fully understood what the underlying organizational mechanism is, that establishes these co-varying regions.

This phenomenon was initially presented in the visual system, where the volume of segments in this system (e.g. primary visual cortex, lateral geniculate nucleus, and optic tract) displayed covariance across subjects (20). Structural covariance can also be found in other highly connected areas, such as the language (21) and memory area (22). This could

suggest that areas that share a behavioral or cognitive function structurally co-vary. Which makes sense as these regions have strong WM tract connections and are activated together. Along with physically and functionally connected regions, areas that share developmental pathways indicate structural covariance (23). Structural covariance is not a uniquely human network, as it has been found in macaques (24) and mice (25, 26). Therefore, in summary structurally co-varying regions reflect some sort of underlying organization. Whether that be structural, functional, developmental or due to genetic factors (18).

Non-Negative Matrix Factorization

A popular method to uncover structural co-variance regions is by extracting components or factors that describe a portion of the variance in the data. This represents a data reduction problem, where the variance within a dataset is reduced to a small number of components that can explain this variance. In the case of brain region structural covariance, the GMV data acquired from VBM preprocessing is reduced to a small number of factors that represent structurally co-varying GM regions.

Non-negative matrix factorization (NNMF) has been proposed as the method of choice for component based GM structural co-variance extraction (26). NNMF is an unsupervised, learning method where the elements of the factorization are held to the restraint of having non-negative values (27). This non-negative constraint leads to a parts based representation of the data, which means components form an additive representation of the data. As a result, NNMF components are more interpretable compared to common methods such as principle component analysis (PCA) and independent component analysis (ICA) (27). Neuroimaging data analysis by NNMF has also lead to more interpretable results in deriving structurally co-varying GM regions in adults (26) and adolescents (28) and when using GMV for age prediction (29). The utilization of NNMF on human neuroimaging data is reasonable well documented, but less is known if it could be applied with the same success to non-human primates

Aim and Objectives

There is no chimpanzee template and pre-processing pipeline openly available to the scientific community. As Chimpanzees are humans closest extant relative they offer an exciting opportunity to further understand the evolutionary development of the human brain. Therefore, the aim of this study is to propose a chimpanzee specific pre-processing pipeline and demonstrate its viability in chimpanzee brain morphometry research. An outline of the steps involved to create with species specific anatomical template, DARTEL/Shooting templates and TPM is provided so it can be used by the wider scientific community. The pipeline is accessible for the freely available Statistical Parametric Mapping (SPM) toolbox Computational Anatomy Toolbox (CAT12). Utilizing the newly created high contrast anatomical chimpanzee template, proposed annotations of major macroanatomical structures is given, referred to as 'DaVi' Labeling.

Evaluation of the processed images validity will be conducted by replicating previously published results regarding age related neurodegeneration in both chimpanzees and humans. GMV decline during aging is a robust and well researched process that was chosen as the test parameter. Corresponding with the human and chimpanzee literature, the hypothesis that there will be a significant decline in GMV in response to aging and that this atrophy will be mostly evident in the frontal and temporal cortex. Sex differences will also be explored, in particular using VBM as this has not been done before.

The final aim of this study is to show initial findings of a data driven brain parcellation using NNMF structurally co-varying GM regions. This unsupervised learning algorithm has been shown to produce biologically interpretable parts based parcellations of the human brain (26, 28, 29). However this technique has not been tested in chimpanzees and could open the door to intriguing interspecies brain structure and organization comparisons.

Methods

Subjects

The structural T1-weighted MRI scans of 219 captive chimpanzees (pan troglodytes), 134 females and 85 males were used in this study. The chimpanzees were held at two different locations; 135 housed at the National Center for Chimp Care of The University of Texas M.D Anderson Cancer Center (UTMDACC) and from 84 chimpanzees being housed at the Yerkes National Primate Research Center (YNPRC) which works in association with Emory University in Atlanta, Georgia. These scans are publicly available at http://www.chimpanzeebrain.org (NIH grant NS092988). The age of the chimpanzees at the time of their MRI scans ranged from 8 – 53 years old (M = 27.04, SD = 6.74).

Image Collection Procedure

The MRI scans of the chimpanzees all followed standard procedures at the YNPRC and UTMDACC which are designed to minimize stress (30). *In vivo* scanning was conducted during one of their annual examinations. Each animal was sedated with ketamine (10 mg/kg) or telazol (3-5 mg/kg) and next were anaesthetized with propfol (40-60 mg/kg/h). The YNPRC subjects were then transported to the MRI facility and the UTMDACC subjects were wheeled to the mobile imaging unit. The subjects remained anaesthetized during the scanning period and the transport time it took to move them from their housing cages to the imaging facility and back. Within the MRI scanning facility, the subjects were placed in a supine position in the scanner with their head fitted to a human-head coil. The duration of the scan ranged from 30-60 minutes depending on brain size. Upon completion, the chimpanzees were briefly singly-housed for 2-24 hours to enable close monitoring and safe recovery from the anesthesia prior to returning to their home social group. All procedures were approved by the Institutional Animal Care and Use Committees at YNPRC and UTMDACC, also following the guidelines of the Institute of Medicine on the use of chimpanzees in research.

76 chimpanzees were scanned using a 3.0 Tesla scanner (Siemens Trio, Siemens Medical Solutions USA, Inc., Malvern, Pennsylvania, USA). T1-weighted images were collected using a three-dimensional gradient echo sequence (pulse repetition = 2300 ms, echo time = 4.4 ms, number of signals averaged = 3, matrix size = 320 × 320, with 0.6 × 0.6 × 0.6 resolution). The additional 143 chimpanzees were scanned using a 1.5T G.E. echo-speed Horizon LX MR scanner (GE Medical Systems, Milwaukee, WI). T1-weighted images were collected in the transverse plane using a gradient echo protocol (pulse repetition = 19.0 ms, echo time = 8.5 ms, number of signals averaged = 8, matrix size = 256 × 256, with 0.7 × 0.7 × 1.2 resolution).

DICOM to NIfTI conversion

T1-weighted MRI scans produce images in the form of DICOM's (Digital Imaging and Communications in Medicine) which need to be converted into NIfTI's (Neuroimaging Informatics Technology Initiative) to enable easy processing and analyses. NIfTI's are extensively used as the preferred image file format for MRI analyses which is used so commonly because it relates voxel index (i,j,k) to spatial location coordinates (x,y,z) enabling easy analyses. MRI scans are saved as a file format called DICOM by the scanner. Converting DICOM's to NIfTI's is achieved using the program 'dcm2nii' from mricron (http://people.cas.sc.edu/rorden/mricron/index.html).

Image processing

Image processing is a very computationally heavy endeavor which can be handled by modern computers. The software program SPM12 (v6685) (https://www.fil.ion.ucl.ac.uk/spm/software/spm12) and the toolbox, CAT12 (r1278) (http://dbm.neuro.uni-jena.de/cat) were used for image processing. Both are run using the computing environment and programming language MATLAB (version 8.3 R2014a).

Noise and Bias Correction

The initial step for CAT12 preprocessing is for the single subject scans to be cleaned of noise and signal inhomogeneity created by the MRI scanner. Images attained from MRI scanners usually contain random noise from the acquisition process, which can introduce problems in subsequent preprocessing steps. CAT12 uses a specific denoising filter, spatial adaptive non-local-means (SANLM) to remove this noise (31). SANLM filter can remove the noise while managing to keep the image edges. Signal inhomogeneity is another unavoidable scanner problem that needs to be corrected. This is where the image intensity is not uniform across the entire brain due to variations of the magnetic field and not anatomical differences. WM can then in one area of the brain have the same intensity as GM in another area of the brain. To correct for signal inhomogeneity an algorithm in SPM models smooth intensity variation by a linear combination of discrete cosine transform basis functions (14). Meaning, the image is represented as a sum of sinusoids of varying magnitude and frequency. As the image inhomogeneities have low frequencies, the slowly varying signal inhomogeneities below a certain cut-off threshold can be isolated in terms of discrete cosine transform components.

SPM 12 segmentation and Spatial Registration

To analyze anatomical differences in homologous regions across subjects, all subjects images need to be brought into a common anatomical space. There are several ways this can be achieved, SPM12 does this by matching the different tissue types within the subjects brain to the same tissue type within a template. Therefore, the individual scans need to be segmented into GM, WM, and CSF tissue segment maps. To extract the GM, WM, and CSF tissue segments one requires a TPM. The TPM gives a probability density of a tissue type contained within a voxel. Probability is determined by a Gaussian mixture model (32). The model combines two or more Gaussians that indicate image intensity distribution for each tissue type. Once these segment maps are established they are non-linearly deformed to the segments of the TPM. This means each voxel is deformed to the shape of the TPM, which puts all images into a common anatomical space and gives the deformation field of Jacobian determinants for each subjects segments.

CAT12 Specific Preprocessing

CAT12 improves upon the tissue classification and segmentation conducted by SPM12. CAT12 fulfills this process by utilizing several techniques, such as Local Adaptive Segmentation (LAS), partitioning, brain extraction, Adaptive Maximum A Posterior (AMAP) segmentation and finally cleanup (fig. 2). LAS is applied in order to counteract the varying GM intensities of different regions. Regions such as the motor cortex, basal ganglia, and occipital lobe have increased myelination and iron content (33). This can lead to an underestimation of GMV within these regions. Therefore, a local intensity transformation of all tissue types is employed to reduce these effects. The CAT atlas is spatially adapted to the individual brain which improves segmentation and is needed for brain extraction, partitioning, and cortical surface reconstruction. This atlas is a map of major brain regions such as the hemispheres, basal ganglia, ventricles, and cerebellum. Brain extraction and partitioning is important to ensure further processing and analysis is conducted only on brain tissue. A graph cut method and region growing routines are conducted during brain extraction and partitioning to improve the brain mask (34). The final segmentation approach, AMAP doesn't use the TPM as in classical SPM12 segmentation. It doesn't need the a priori information on the tissue probabilities from the TPM. Instead AMAP models the variation of the parameters as slowly varying spatial functions (35). This can then account for intensity inhomogeneities and local intensity variations. Finally CAT12 includes a cleanup routine that uses morphological, distance and smoothing operations to remove remaining meninges after the final segmentation.

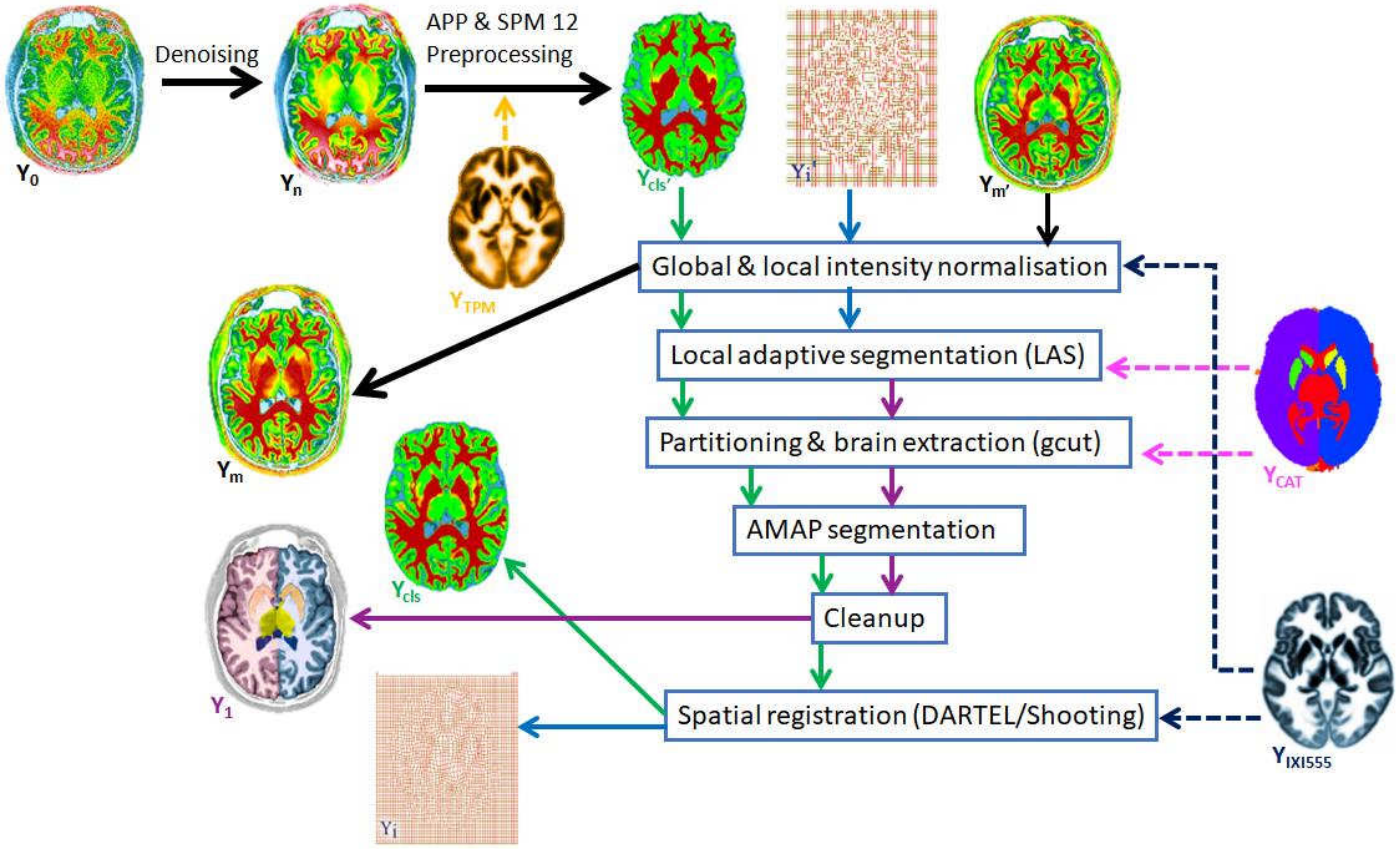

Figure 2. A diagram of the CAT12 preprocessing pipeline. It begins with SANLM denoising followed by affine preprocessing (APP) and initial SPM12 preprocessing and segmentation based on the SPM12 TPM (Y_{TPM}). This creates a tissue classification map ($Y_{cls'}$), Jacobian determinants map ($Y_{i'}$) and normalized image ($Y_{m'}$). $Y_{m'}$ is further refined by global and local normalization with the help of the IXI555 template (Y_{IXI555}) to produce the final normalized image (Y_m). Y_i' is used to map an atlas (Y_{CAT}) to the individual space (Y_1) which is important for local adaptive segmentation (LAS) graph cut brain extraction (gcut) and surface reconstruction. Following brain extraction $Y_{cls'}$ the Adaptive Maximum A Posterior (AMAP) is used to create a priori independent segmentation that is further corrected by a cleanup routine to remove blood vessels and meninges. Finally $Y_{cls'}$ is used for DARTEL/shooting registration to the Y_{IXI555} template to create the final tissue classification (Y_{cls}) and Jacobian map (Y_i). This diagram was adapted from the work done by (36)

DARTEL / Geodesic Shooting Registration and normalization

The final step for MRI preprocessing is spatial registration and normalization (fig. 2). DARTEL (37) and optimized geodesic shooting (38) are bread from the field of computational anatomy. These algorithms use a specific type of transformation called diffeomorphism. DARTEL/Shooting registration utilizes the technique of large deformation diffeomorphic

metric mapping (LDDMM) which manages a larger deformation as a sequence of smaller ones (39). This works in neuroimaging by individual GM and WM segments being simultaneously warped to the GM and WM segments of the DARTEL/shooting templates of increasing registration accuracy in an iterative fashion. In order to preserve regional volume amounts within the tissue the warped images are multiplied by their Jacobian determinants, this is called modulation. As the Jacobian determinants encode the relative tissue volume, both before and after warping individual differences can be conserved. This is completed in terms of intensity so if a particular region has been shrunk by half through warping then the intensity of that region will be doubled.

Chimpanzee TPM and Shooting Templates

Before the creation of a chimpanzee template and properly preprocess the individual images can be conducted, chimpanzee specific TPM, DARTEL/shooting templates (38), and a CAT atlas (fig. 3) need to be established. This initial step uses the CAT12 ”greater_ape” setting (40). This setting uses the work generated by (2) on the structural brain MRI scans of various greater ape species to establish greater ape TPM and shooting templates. Initially all structural T1 images are segmented into GM, WM, and CSF and spatially registered using the greater ape TPM. The rigid body and affine registered outputs are then saved. These outputs can consequently be affine and non-linearly registered to 6 greater ape DARTEL/shooting templates in an iterative fashion. After each iteration the resulting tissue maps were averaged and smoothed (2mm kernel), which results in 5 chimpanzee specific DARTEL/shooting templates to be generated. These shooting templates are then averaged to include both the affine only normalized, as well as the fine non-linear registered maps to establish the chimpanzee specific TPM. Finally, the CAT atlas has to be manually adapted to the chimpanzee TPM. To produce the chimpanzee specific CAT atlas which aids in segmentation, brain extraction, and is crucial for surface reconstruction.

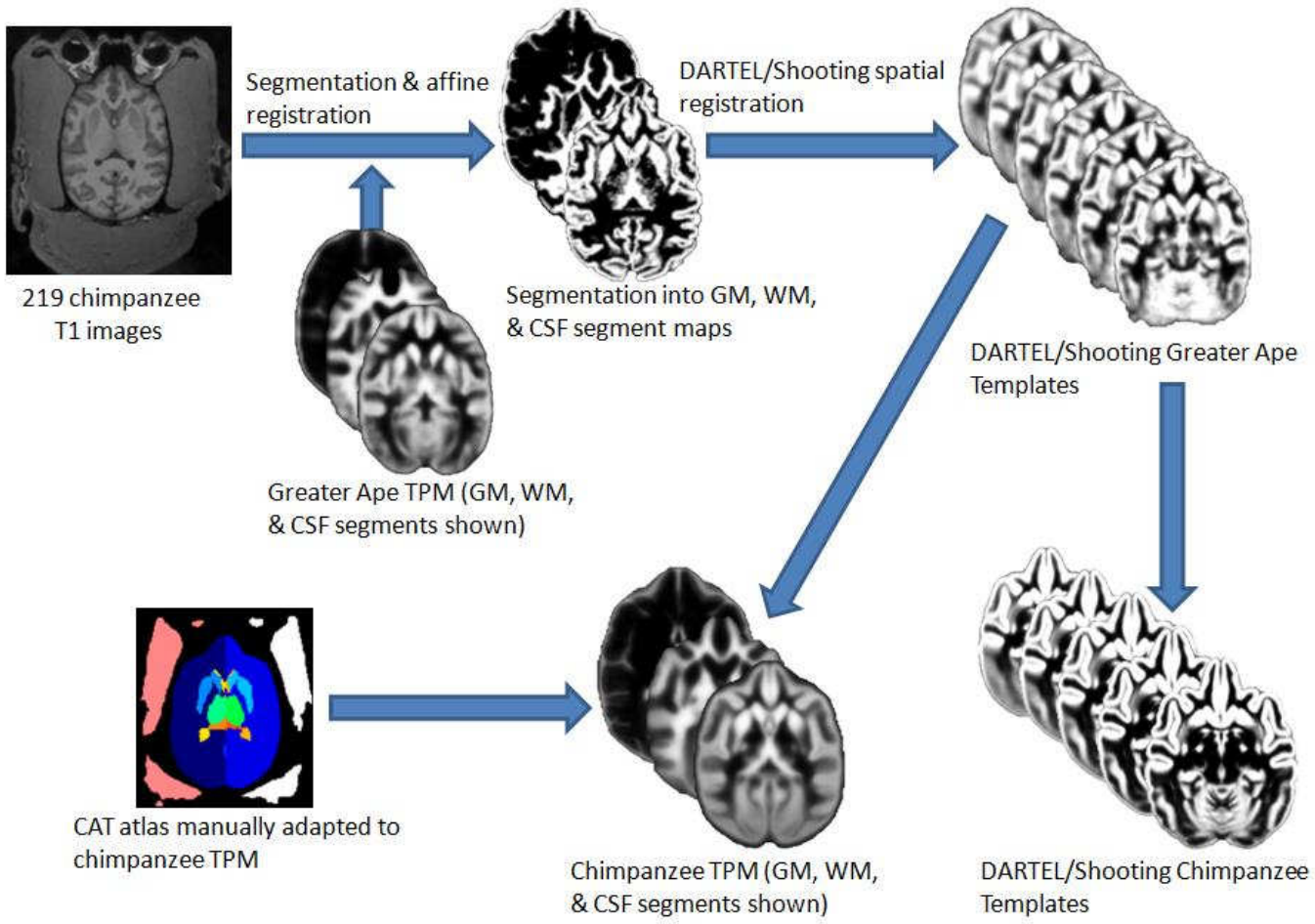

Figure 3. A diagram of the pipeline to create chimpanzee specific TPM, DARTEL/Shooting templates, and CAT atlas which are all required for CAT12 preprocessing. The 219 individual chimpanzee T1 images initially go through segmentation and affine registration using the Greater Ape TPM(2). GM, WM, and CSF segment maps are created and then each tissue type segment is DARTEL/Shooting (37, 38) spatially registered to the corresponding tissue type in the 6 Greater Ape DARTEL/Shooting templates of increasing registration accuracy in an iterative fashion. This produces the chimpanzee specific DARTEL/Shooting templates and TPM. Finally the CAT atlas is manually adapted to chimpanzee TPM to establish a chimpanzee specific CAT atlas.

Chimpanzee Template and Preprocessed Images

With the newly created species specific DARTEL/shooting templates, TPM and CAT atlas then CAT preprocessing could be conducted and the creation of chimpanzee template could be undertaken (fig. 4). This entails facilitating segmentation and spatial registration with the chimpanzee TPM on the same sample used for the creation of the TPM and DARTEL/shooting templates. The segmentation is also benefited by the help of the newly

adapted chimpanzee CAT atlas. The segments of each chimpanzees image goes through DARTEL/shooting registration and these registered images are then averaged to form the chimpanzee template. With all the species specific templates, TPM and atlas, effective preprocessing on the chimpanzee sample using the CAT preprocessing pipeline can be conducted in an effective manner.

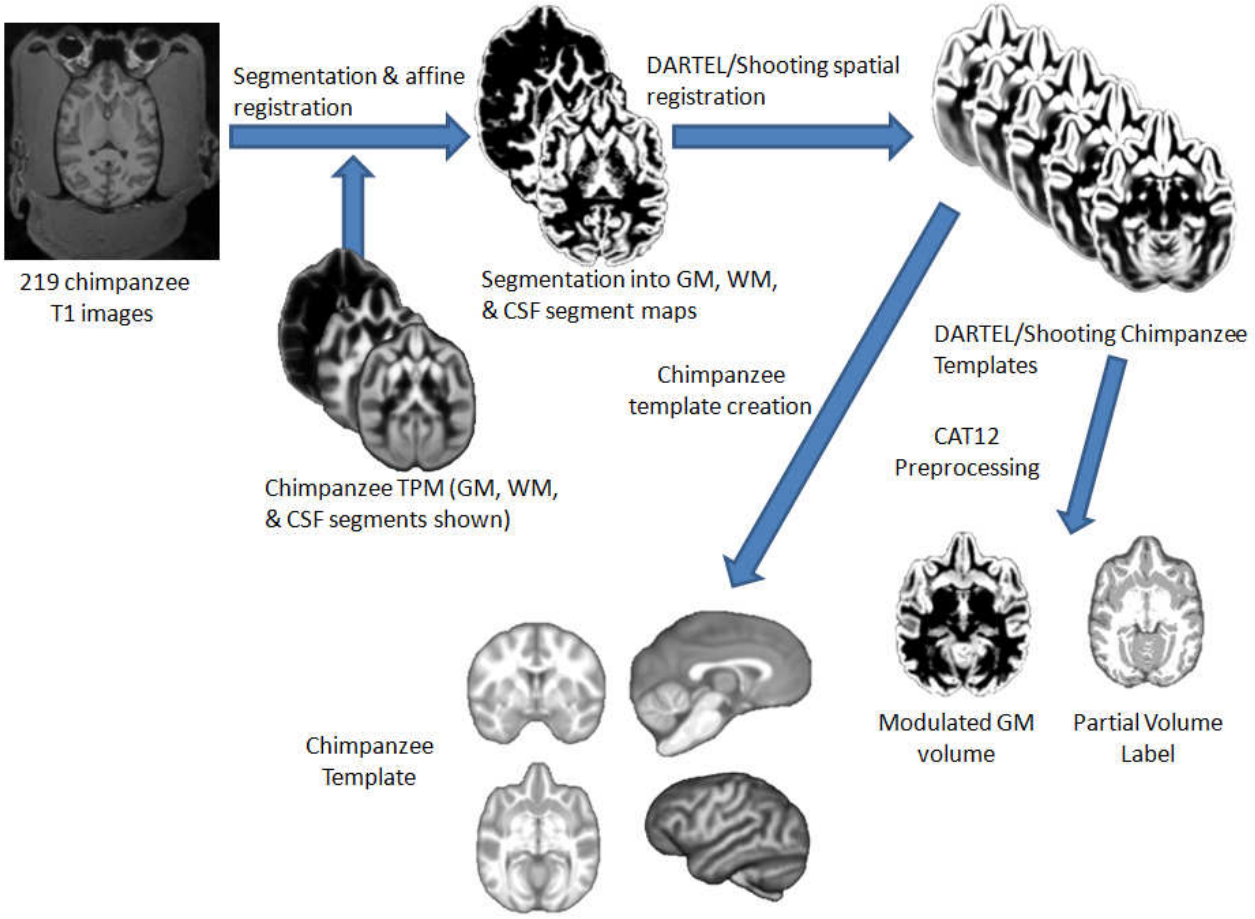

Figure 4. A diagram of the pipeline to create the chimpanzee template and preprocessed images. The 219 individual chimpanzee T1 images got through the same process as described in figure 3 but this time with the newly created chimpanzee specific TPM and DARTEL/Shooting templates. Averaging all the spatially registered images then produces the chimpanzee template. CAT12 preprocessing is also conducted using the chimpanzee specific templates which produces, for example modulated GM maps and partial volume labels for each subject.

DaVi Labeling

The newly created template enabled annotation of the major macro-anatomical structures within the chimpanzee brain. Identification of the major macro-anatomical structures was done manually using the program 3D Slicer (https://www.slicer.org). The segmentation function within Slicer 3D enables the user to paint areas of the image within the 3 planes (coronal, axial, and sagittal) and view the segmentation in 3D. This 3D option was very helpful function, as one can view the slices as a projected volume which makes it much easier to distinguish the different areas. This function was used to paint the major GM structures within the left cerebrum and cerebellum hemisphere, then flip this segmentation onto the right hemisphere. Afterwards annotation of the corpus callosum, anterior commissure, ventricles (lateral, 3rd, and 4th), optic nerve/chiasm, and the major structures of the brain stem was conducted.

Determining the location of the structures was conducted by consulting several different resources. Differentiation of the various cortical structures was based on the major gyri that could be located on the chimpanzee template. The border of two gyral structures was set at the midpoint of the connecting sulcus. This was decided as the arbitrary border as one must go to the microanatomical scale to determine the exact border of two areas within a sulcus. As a base for annotations, initial consultation of the Desikan-Killiany atlas (41) was done as it is a well established human macroanatomical atlas and has also been used in a study comparing the gyrification and cortical thickness of humans and chimpanzees (42).

Human microanatomical atlases (43, 44) were examined to better understand the location of particular gyri and deep brain structures. Human brain atlases were the main resource utilized as the major macroanatomical structures are very similar between humans and chimpanzees. Some large gyral structures were subdivided into 2 or 3 parts. This was done with an ambiguous cut to separate the area into 2 or 3 equal parts. These areas include the; Superior Frontal Gyrus (3P), Middle Frontal Gyrus (2P), Inferior Frontal Gyrus (3P), Orbito-frontal Cortex (2P), Pre- and Post-central Gyrus (3P), Superior Temporal Gyrus (2P), Middle Temporal Gyrus (3P), and Inferior Temporal Gyrus. Easily identifiable non-GM structures were annotated, such as the corpus callosum, anterior commissure, ventricles (lateral, 3rd, & 4th), optic nerve and chiasm, mesencephalon, pons, and medulla oblongata. The labeling

was confirmed by Robert Dahnke from the University of Jena. Enabling a second opinion on the parcellation and he also annotated the sub-regions within the cerebellum in consultation with the work of (45).

Image Quality Control

Quality control (QC) was conducted on the raw NIfTI images and the final preprocessed normalized images. Prior to preprocessing visual inspection of the raw images was conducted to identify any large deformations or artifacts, but none were found. The built-in QC function in CAT12 to evaluate which images were of a good enough quality to be used in subsequent analysis. CAT12 QC is a retrospective empirical quantification of the image quality before CAT12 preprocessing. Each image is given a ranking depending on three criteria, noise contrast ratio, inhomogeneity contrast ratio, and resolution. The resulting ratings are then combined to produce a weighted average image quality rating (IQR). A pdf is created for all subjects that contains a percentage rating (0-100%) and a corresponding letter value (F - A+) for noise, bias (inhomogeneity), resolution and IQR. Arbitrarily an image was classified as to fail QC if it had a noise grade less than or equal to ”C” (70%) and a total (IQR) grade of less than ”B”(80%). This cut-off was applied to insure high quality images be used for analysis as low quality images can lead to GM underestimations in preprocessing (46).

Visual inspection of the QC passed normalized preprocessed images was conducted. This entailed examining each image for failed/incorrect segmentation, large GM underestimations, or large structural deformations. A graphical representation of the age range of the chimpanzees whose images passed QC can be seen in figure 5. The number of QC passed images that were analysed in each of these groups are: 70 3T (49 females, 10 - 54 y/o, M = 25.38, SD = 11.28), 55 1.5T (37 females, 11 - 44 y/o, M = 26.16 , SD = 8.29), and 125 total (87 F, 10 - 54 y/o, M = 25.81, SD = 10.03).

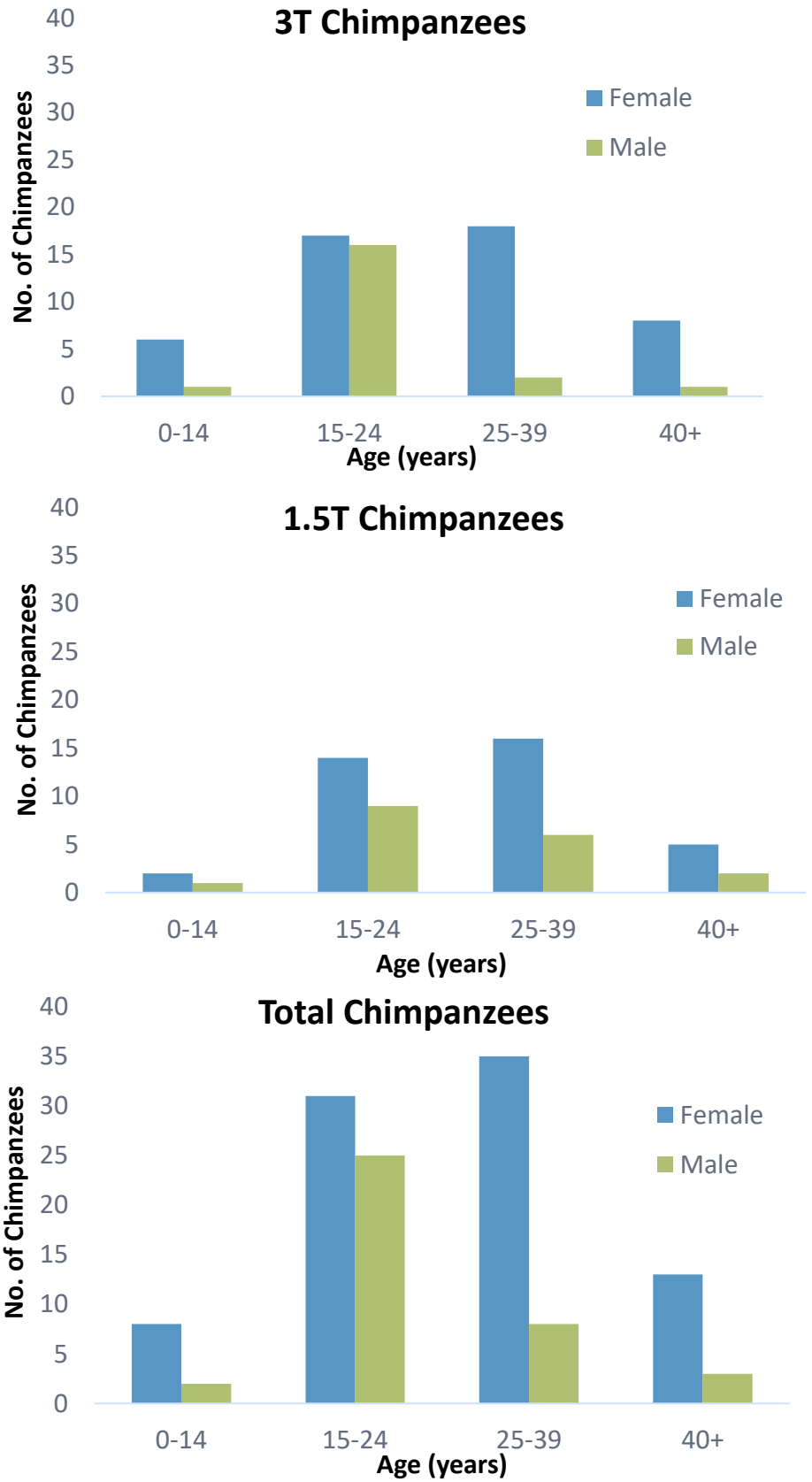

Figure 5. Histograms indicating the number of images in each age range that passed QC in the 3T (top), 1.5T (middle), and total (bottom) samples. These are ranges were chosen as they represent adolescence, early adulthood, adulthood, and elderly respectively.

Gray Matter Atrophy in During Aging

To analyse the effect aging has on GMV three approaches were taken; a regression model of GMV against age, a average ROI GMV against age regression model, and finally a VBM analysis of GMV decline in response to aging. For each approach the analyses was broken up into 3 parts. These were all QC passed 3T images, 1.5T images and the total of both scanners.

Total Gray Matter Age Regression Model

Determination of total GM atrophy over the chimpanzee lifespan was conducted using a linear regression model. To extract the total GM volume for each chimpanzee the CAT12 estimate TIV (Total intracranial Volume) function was used. This enables the user to obtain the total GM, WM, CSF, WMH (White Matter Hyper-intensities), and TIV from the XML (Extensible Markup Language) files produced form the CAT12 preprocessing. These measurements are taken from the normalized preprocessed images. Variation in head size was accounted for by expressing GM volume as a percentage of TIV. The software environment R (version 3.5.0) was used was used for the statistical regression modelling. The R function 'lm' was employed for the linear model. The dependent variable within the model is the percentage GM of TIV and the independent variable was age with sex as a covariate and for the total sample sex and scanner strength were covariates. R^2 was calculated to determine slope and p-value ($p \leq 0.05$) was used to determine a significant effect on the independent variable.

Gray Matter ROI Age Regression Model

To extract the ROI's the newly created DAVI Labelling was used. As the DAVI labelling was created in template space it can easily transposed back onto the individual space just like other commonly used human atlases. The CAT12 function 'extract ROI data' was used to extract the average GM volume within the ROI, which was averaged from both hemispheres. Similar as for the total GM regression model, the ROI GM volume was expressed as a percentage of TIV to compensate for varying head sizes. The major ROI's that

were chosen can be seen in Table 2. The regression model was then carried out in the same fashion as in the total GM age regression. With the dependent variable being percentage ROI GM of TIV instead of total GM as a percentage of TIV with age and sex were the independent variables for the 1.5T and 3T samples and scanner was added for the Total sample. P-value was calculated for the effect age had on percentage GM volume of ROI and then corrected for multiple comparisons using FDR ($p \leq 0.05$)(47).

Voxel Based Morphometry

VBM was conducted using the CAT12 SPM12 toolbox. The modulated and spatially normalized GM segments that passed QC were used of the VBM analysis. All images were smoothed with a FWHM (full width half maximum) smoothing kernel of 6mm. Smoothing is important to compensate for slight registration errors and to make the distribution more Gaussian for better interpretable statistical analysis. To establish the model the CAT12 function 'Basic Models'. The same groups were analyzed as with the regression models. The model contained a one-sample t-test with covariates TIV, age, sex and for the total group also scanner. An implicit mask was applied. The rest of the design factors were not changed from standard. VBM was also employed to determine sex differences in GMV in chimpanzees. Age matched groups males and females with the same number of subjects were analyzed within the three samples, 1.5T, 3T, and total. This resulted in 36 1.5T chimpanzees (12 - 41 y/o, M = 24.52, SD = 7.27), 42 3T chimpanzees (11 - 45 y/o, M = 19.89, SD = 5.38), and 78 total chimpanzees (11 - 45 y/o, M = 22.63, SD = 7.42) being analyzed. Within the model TIV was a covariate for all three models and scanner was a covariate for the total sample. All results were corrected by Threshold-Free cluster enhancement (TFCE) with a 60% GM mask and 5000 permutations .Presented Significant clusters are corrected for multiple comparisons with family wise error (FWE) < 0.05.

Non-Negative Matrix Factorization

The uncovering of structurally GM co-varying regions was achieved with the algorithm NNMF. This algorithm was chosen due to its non-negative constraint on all elements which produces parts based representation of the data that facilitates interpretability. NNMF has

previously been shown in humans to extract interpretable and reproducible components (26, 28). NNMF as the name suggests is a matrix factorization algorithm. The algorithm factorizes an input matrix W into two approximation matrices with non-negative elements, W≈XY (fig. 6).

The input matrix contains the dimensions GM voxels (V) within the brain by the number of subjects (N). This information is taken from the modulated processed images from the established chimpanzee preprocessing pipeline. The GM intensity for the voxels was obtained from the registered and normalized GM maps after a GM mask of 0.6 to ensure only GM voxels would be analyzed. The X matrix has the dimensions voxels (V) by the number of components (C), which are predefined by the user. Contained in the X matrix are the loadings of the components for each voxel. The second matrix Y, is of size components (C) by the number of subjects (N) and contains the subject specific weights for each component. This means these weights indicate the contribution of each component in reconstructing the input matrix for each participant. The component loadings were visualized as a 3D rendering of the GM voxels accompanied by three axial volume segments.

Visualization was produced using the MRIcroGL software package (https://mccauslandcenter.sc.edu/mricrogl/home). The same samples used in the GM atrophy age analysis were also employed for the uncovering of co-varying GM region utilizing NNMF. For each sample a 2 component (2C), 6 component (6C), and 12 component (12C) solution are presented on the newly created chimpanzee template. This gives the impression how relatively large NNMF components can align with some known and easily identifiable structures.

Orthonormal Projective Non-Negative Matrix Factorization

A variation of NNMF, called Orthonormal Projective Non-Negative Matrix Factorization (OPNMF) will be used as it is favorable when analyzing neuroimaging data (26). OPNMF is preferable as it positively weights the variables within the data matrix that tend to co-vary, which is the exact aspect of the data matrix one searches for in structural covariance analysis. To summarize the matrix factorization shown in figure 6, firstly X is initialized through non-negative double singular value decomposition (NNSVD) (48). Then X is updated

iteratively with a multiplicative update rule, until it converges to an optimum solution (49), but is constrained by orthonormal projection. Finally, OPNMF projects X onto W to obtain a solution that minimizes the reconstruction error yields, Y. From here on out OPNMF will be referred to as NNMF.

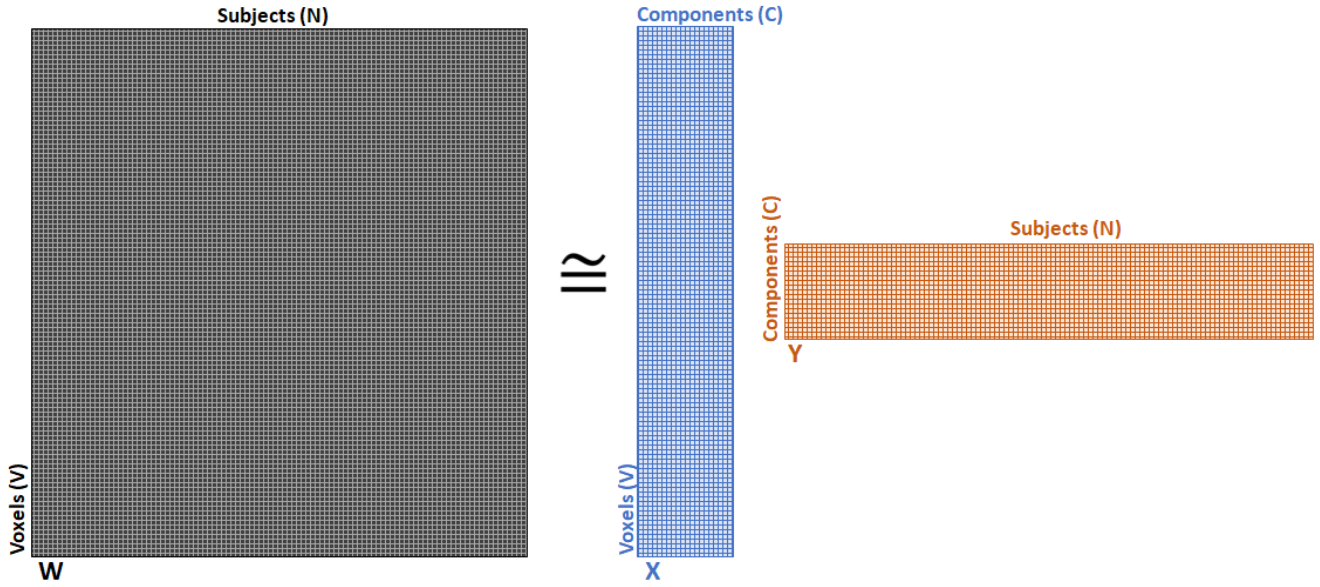

Figure 6. Diagram of matrix factorization employed by NNMF. The matrix W with dimensions number of voxels (V) by number of subjects (N) is factorized using OPNMF into two matrices. Matrix X with dimensions V by the user defined number of components (C) and matrix Y with dimensions C by N. Matrix X is used to present the component solution parcellation of the brain.

Non-Negative Matrix Factorization Quality Control and Smoothing

The signal to noise ratio was too high for extracting solid and useable components, therefore smoothing was required. Spatial smoothing is common practice in VBM analysis and when conducting NNMF on GMV in humans (28, 29). Previous studies in humans had used 8mm smoothing kernels, but as not such research has been conducted on chimpanzee it was decided to try a variety of smoothing kernels to decide which gives the best results. To decide which smoothing kernel best suited a chimpanzee subsample (3T, 1.5T, & Total) NNMF was conducted using 2C, 4C, and 6C solutions with smoothing kernels ranging from FWHM 4mm - 10mm at 2mm intervals for the three samples.

A subjective rating scale was established to determine which smoothing kernel was best suited for each sample. The scale contained rankings from 1-4 which subjectively judge the amount of noise and how solid the components are in the parcellation. Whereby, solid components and little noise means that there is very minimal to no seemingly random dispersion of several voxel components throughout the brain and there are relatively large areas which contain voxels of a single component. The opposite can then be said for a very noisy solution with very few solid components. Visualization of very good and bad judged component solution can be seen in figure 7.

Figure 7. Coronal section from 6 component NNMF of the 3T sample (69 chimpanzees). 4mm smoothing kernel was applied to A and 8mm smoothing kernel was applied to B. A is a representation of a rank 3 (bad) parcellation whereas B is a representation of a rank 1 (good) parcellation. The dark green component in A is dispersed within other components which is undesirable and difficult for interpretation. While B is solid and easily defined components. Red circles highlight the areas in A that are most likely the result of noise and not wanted.

Following the ranking of all component solutions is was found that an 8mm smoothing kernel was optimal for the 3T sample, while a 10mm smoothing kernel was found to be optimal for the 1.5T and total samples.

Results

DaVi Labeling

Visualization of DaVi Labeling of the chimpanzee brain are shown in Figure 8, in the way of lateral, medial, dorsal and ventral aspects. The parcellated areas are given a number within figure 8, which then corresponds to the structures name that can be found in table 1.

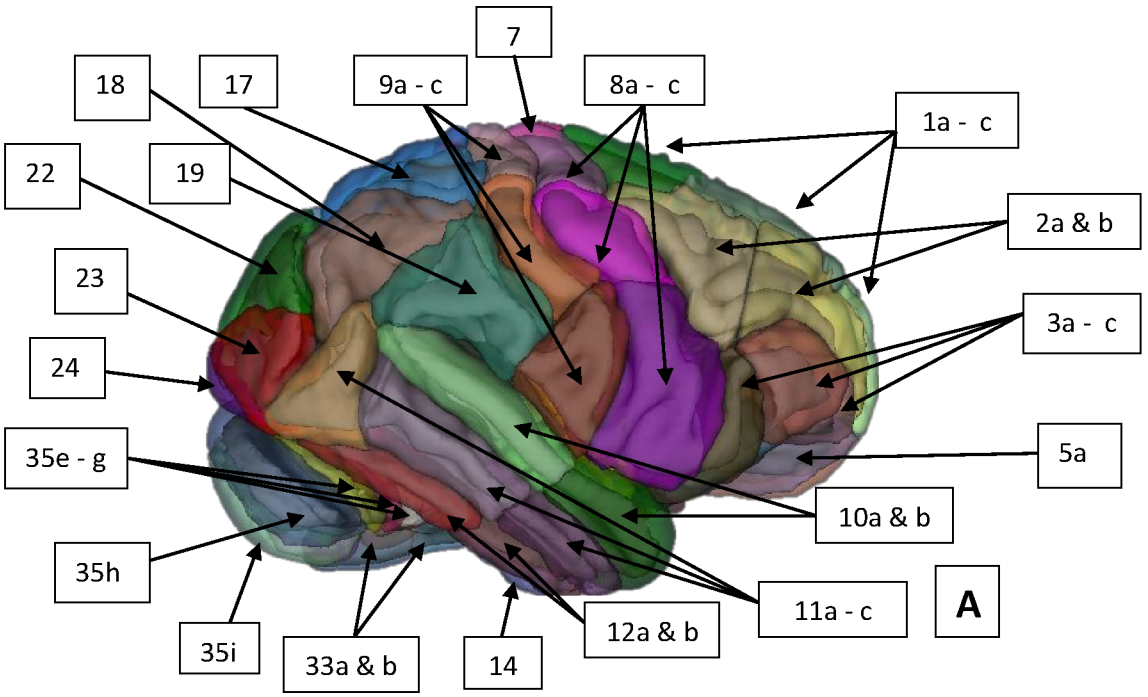

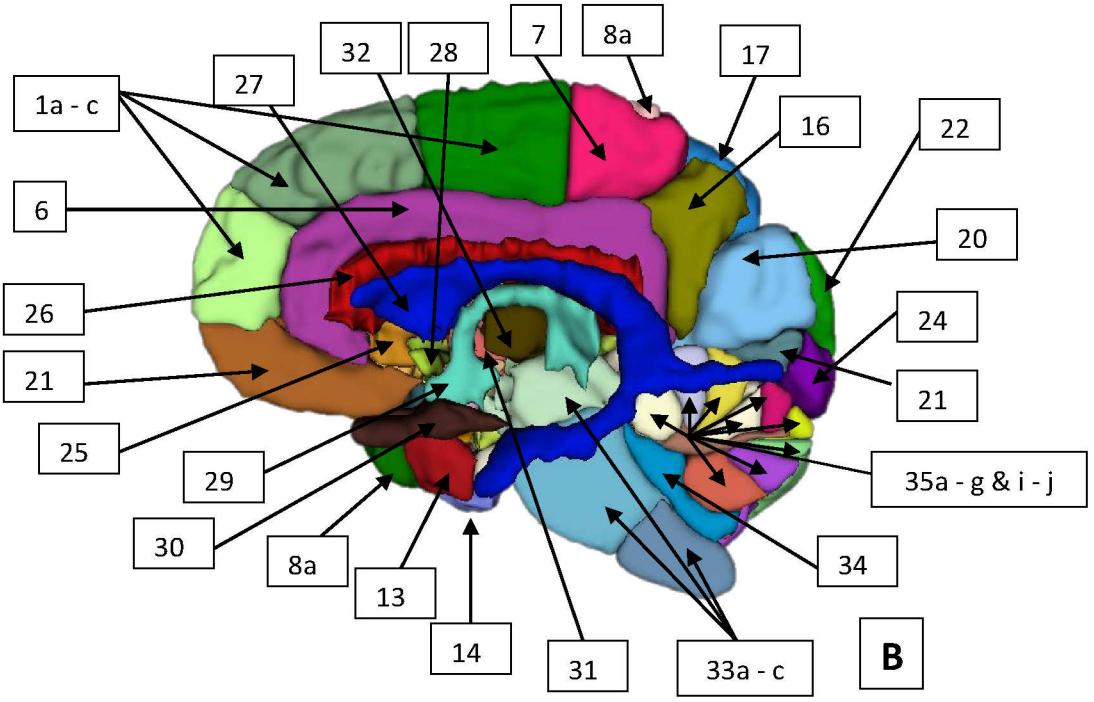
1a - c
27
32
28
7
8a
17
16
22
6
20
26
24
21
21
25
35a - g & i - j
29
30
8a
13
14
31
33a - c
34
B

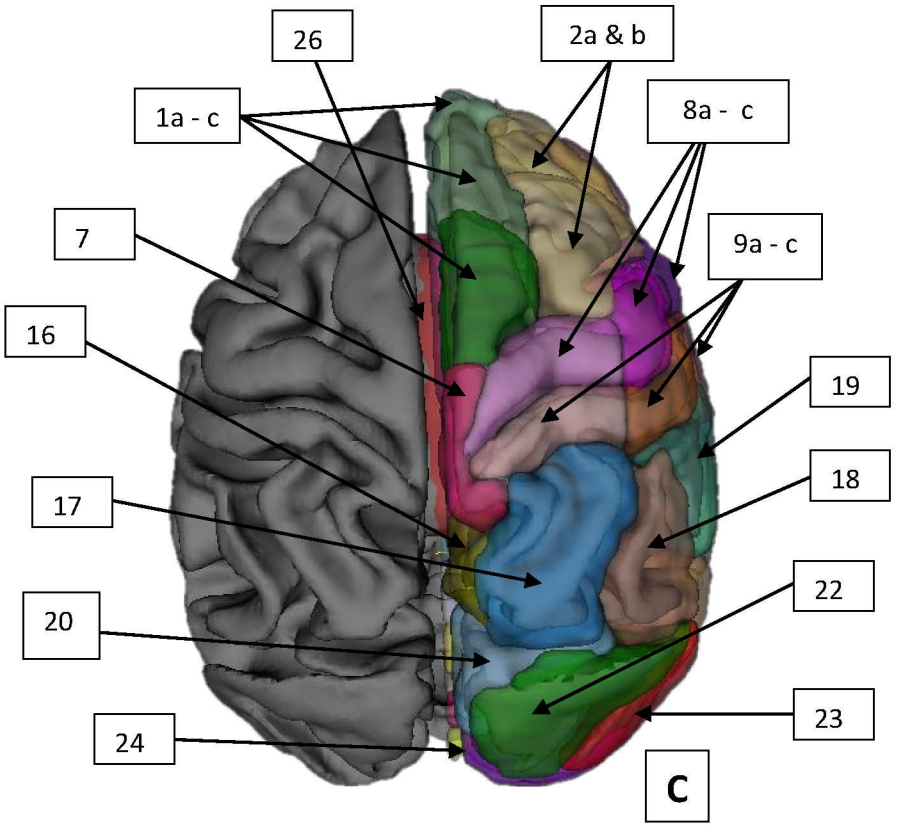
26
2a & b
1a - c
8a - c
7
9a - c
16
19
18
17
22
20
23
24
C

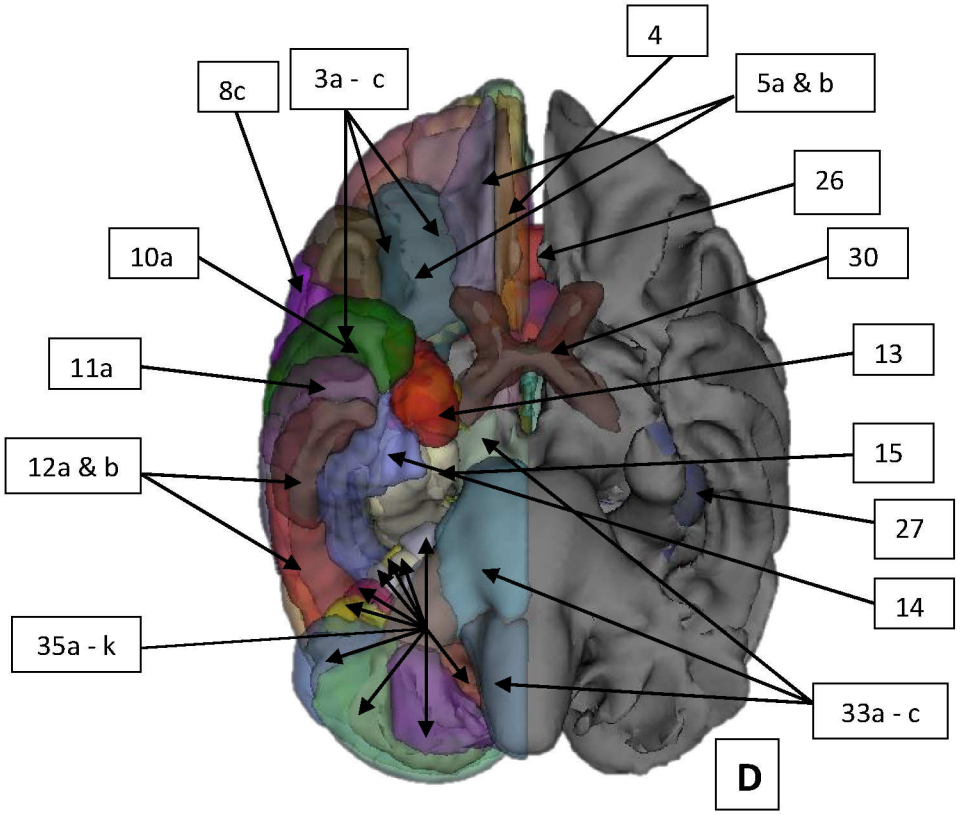

Figure 8. Images of DaVi labeling taken using the Slicer program from the lateral (A), medial (B), dorsal (C), and ventral (D) view of the chimpanzee template. The right hemisphere is labeled while the right hemisphere shows the projected cortical surface. The labeling in A, C, and D is slightly transparent so that the underlying structure can be viewed. Anatomical names corresponding to the numbers can be found in table 1.

Table 1 - The anatomical names for the DaVi labeling annotations in figure 1.

Number	Name of Anatomical Structure
1	**Superior Frontal Gyrus** - a) anterior part & Frontal pole b) middle part c) posterior part
2	**Middle frontal gyrus** - a) anterior part b) posterior part
3	**Inferior Frontal Gyrus** - a) anterior part & Pars Orbitalis b) middle part & Pars Triangularis c) Posterior part & Pars Opercularis
4	**Straight Gyrus**
5	**Orbito-frontal Cortex** - a) medial part b) lateral part
6	**Cingulate Gyrus**

7	**Paracentral Lobule**
8	**Pre-central Gyrus** - a) superior part b) middle part c) inferior part
9	**Post-central Gyrus** - a) superior part b) middle part c) inferior part
10	**Superior Temporal Gyrus** - a) anterior part b) posterior part
11	**Middle Temporal Gyrus** - a) anterior part b) middle part c) posterior part
12	**Inferior Temporal Gyrus** - a) anterior part b) posterior part
13	**Endorhinal Cortex**
14	**Fusiform Gyrus**
15	**Parahippocampal Gyrus**
16	**Precuneus**
17	**Superior Parietal Lobule**
18	**Angular Gyrus**
19	**Supramarginal Gyrus**
20	**Cuneus**
21	**Lingual Gyrus**
22	**Superior Occipital Gyrus**
23	**Middle Occipital Gyrus**
24	**Inferior Occipital Gyrus**
25	**Caudate Nucleus**
26	**Corpus Callosum**
27	**Lateral Ventricle**
28	**Anterior Commissure**
29	**III (3rd) Ventricle**
30	**Optic Nerve/Optic Chiasm**
31	**Globus Pallidus**

32	**Thalamus**
33	**Brain Stem** - a) Mesencephalon b) Pons c) Medula Oblongata
34	**IV (4th) Ventricle**
35	**Cerebellum** **Anterior Lobe** - a) Cerebellum II b) Cerebellum III c) Cerebellum III d) Cerebellum IV e) Cerebellum V lobe A f) Cerebellum V lobe B **Superior Posterior Lobe** - g) Cerebellum VI h) Cerebellum VIIA Crus II of Ansiform lobule i) Cerebellum VIIA Cris I of Ansiform Lobule **Inferior Lobe** - j) Cerebellum VIIIAB k) Cerebellum IX

Note: Annotated structures that cannot be seen in Figure 8 - Insula, Putamen, Hippocampus, Amygdala, and hypothalamus

Total Gray Matter Atrophy during Aging

The initial model established was a multiple linear regression model with percentage GM as the dependent variable and age, sex, for the 1.5T and 3T sample and scanner in the total sample as independent variables. Within the total sample age, sex, and scanner each had a significant effect on GMV decline during aging, $p < 0.001$, $p = 0.003$, and $p < 0.001$ respectively. The overall model was also significant ($p < 0.001$, $R^2=0.74$). The 1.5T sample linear model yielded an overall significant effect on percentage GM ($p<0.001$, $R^2=0.34$), with both age ($p<0.001$) and sex ($p=0.04$) having a significant effect on GMV. For the 3T imaged chimpanzees, the linear model was also overall significant ($p=0.01$, $R^2=0.1$), with age and sex having similar significant effect on percentage GM, $p=0.01$ and $p=0.03$ respectively. The simple linear model of the effect age has on percentage GM produced a significant result for the 3T ($p=0.04$, $R^2=0.06$) and 1.5T ($p<0.001$, $R^2=0.29$) sub-groups and also for the whole sample ($p<0.01$, $R^2=0.05$)(fig. 9).

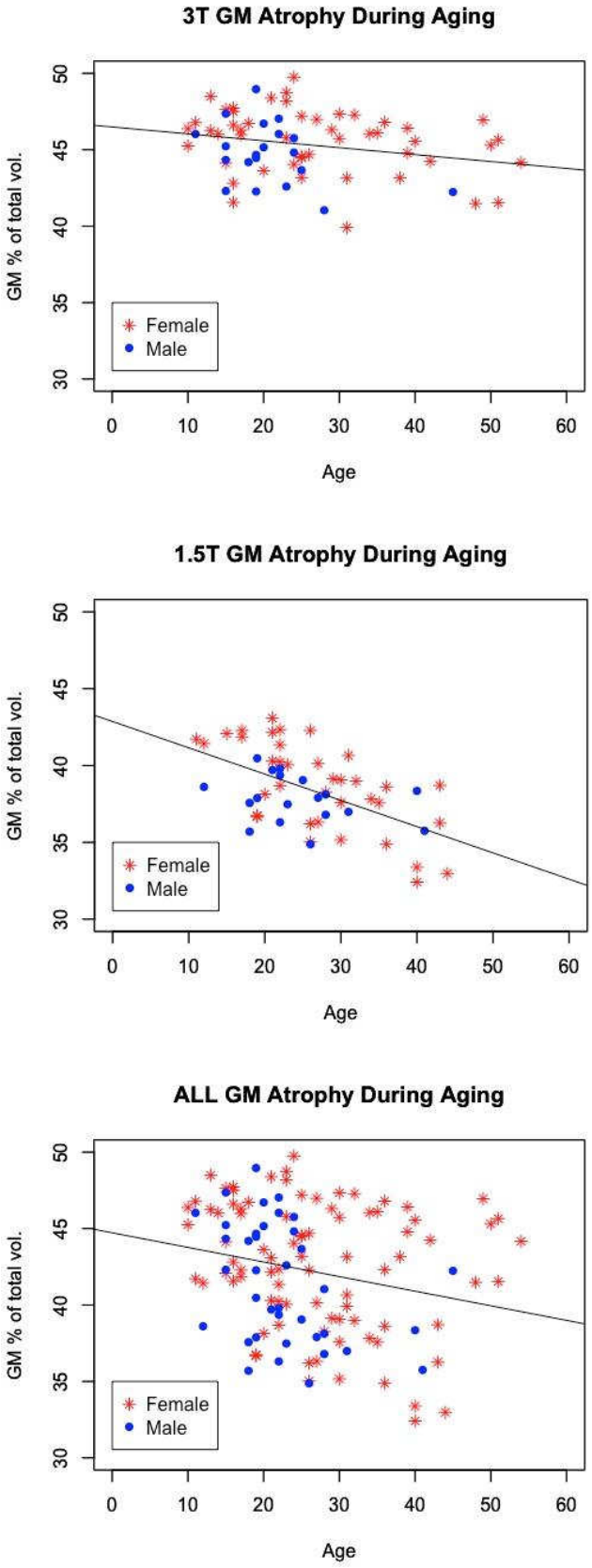

Figure 9. Scatter plots of 3T (top), 1.5T (middle), and total (bottom) chimpanzee samples. Black line represents the linear relationship of the two variables.

ROI Regression Models

The DaVi Labeled ROI's show that there are large differences between the brain areas in regards to how many ROI's display a significant age effect on GMV within each area. The frontal cortex (12/15 = 80%), basal ganglia (8/12 = 67%), and the temporal lobe (17/30 = 57%) all show a higher proportion of ROI's that have a significant age effect after correcting for multiple comparisons (table 2).

Table 2. Aging effect on ROI GMV atrophy

ROI's are organized into brain regions. Significant results are FDR corrected ($p \leq 0.05$). The marking n.s. means a non-significant result at $p \leq 0.05$. and * means a significant decline in GMV due to aging at $p \leq 0.05$.

Frontal Cortex & Cingulate Gyrus			
ROI Name	**3T**	**1.5T**	**Total**
Superior Frontal Gyrus	n.s.	*	*
Middle Frontal Gyrus	n.s.	*	n.s.
Inferior Frontal Gyrus	*	*	*
Lateral Orbito-frontal cortex	*	*	*
Medial Orbito-frontal Gyrus	*	*	*
Cingulate Gyrus	n.s.	*	*
Motor Cortex			
Pre-central Gyrus	n.s.	*	n.s.
Post-central Gyrus	n.s.	*	n.s.
Paracentral Lobule	n.s.	n.s.	n.s.
Temporal Lobe			
Superior Temporal Gyrus	n.s.	*	*
Middle Temporal Gyrus	n.s.	*	*
Inferior Temporal Gyrus	*	*	*

Entorhinal Gyrus	n.s.	*	n.s.
Insula	n.s.	*	n.s.
Parahippocampal Gyrus	n.s.	n.s.	n.s.
Fusiform Gyrus	*	*	*
Lingual Gyrus	*	*	*
Amygdala	n.s.	*	*
Hippocampus	n.s.	n.s.	n.s.
Parietal & Occipital Lobe			
Superior Parietal Lobule	n.s.	*	n.s.
Supramarginal Gyrus	n.s.	*	*
Angular Gyrus	n.s.	n.s.	n.s.
Superior Occipital Gyrus	n.s.	n.s.	n.s.
Middle Occipital Gyrus	n.s.	n.s.	n.s.
Basal Ganglia			
Caudate Nucleus	*	*	*
Putamen	n.s.	*	*
Globus Pallidas	*	n.s.	*
Thalamus	n.s.	*	n.s.

Grey Matter Atrophy VBM

The TFCE VBM (FWE<0.05) the QC passed 3T images (fig. 10) yielded less significant clusters compared to the total and 1.5T sample. Figure 10a and C indicate small clusters at the posterior part of the right superior temporal gyrus and at the inferior and orbito part of the left frontal cortex respectively. When looking at the internal structures (fig. 10c) there are significant clusters at the Caudate Nucleus, Putamen, and cuneus.

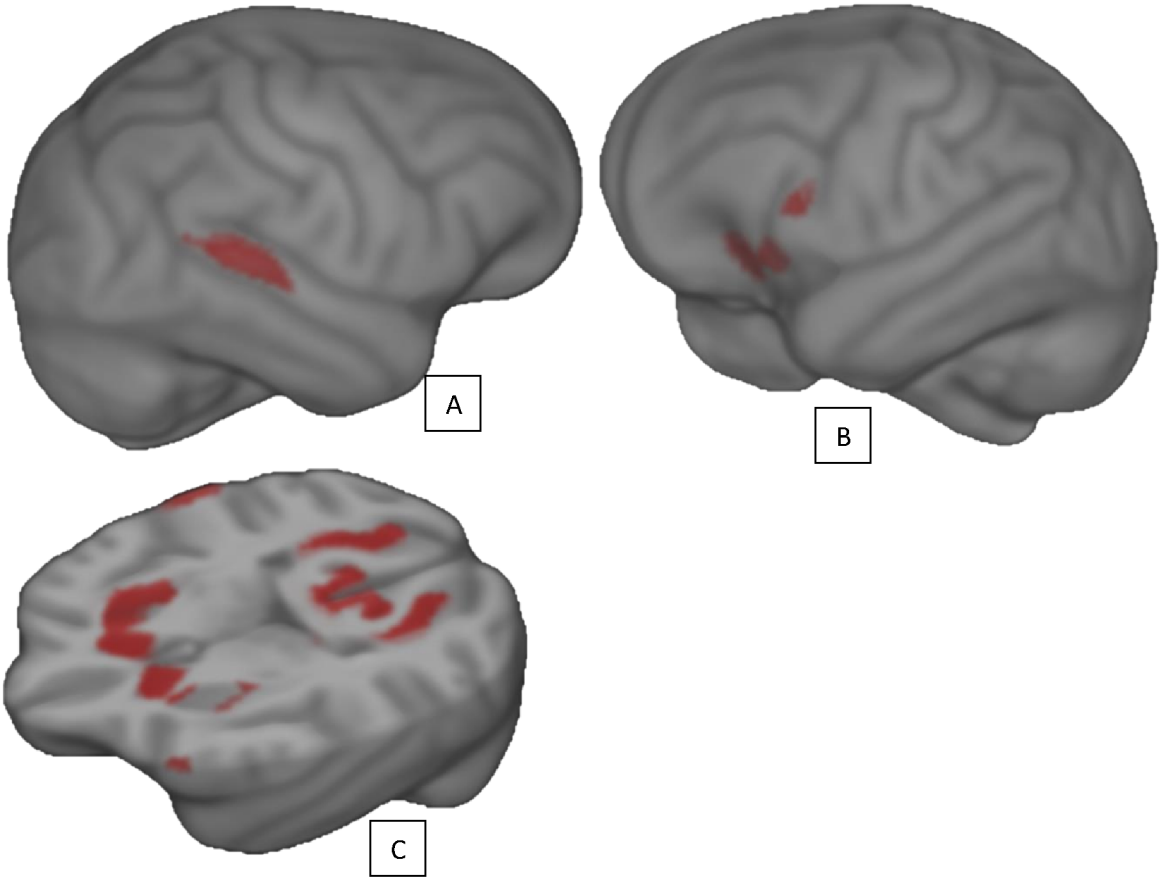

Figure 10. TFCE VBM (FWE<0.05) results from the 3T imaged sample of QC passed chimpanzees. Significant clusters indicate GM atrophy during aging. Clusters are presented a 3D rendering of the chimpanzee template. A shows the right lateral side of the brain, B shows the left lateral side of the brain, C shows the internal aspect of the brain.

The TFCE VBM (FWE<0.05) the QC passed 1.5T images (fig. 11) show a similar cluster pattern as the total sample. Whereby, the right hemisphere (fig. 11a) has a large cluster that runs the length of the posterior part of the temporal lobe into the parietal cortex. Another large cluster can be seen at the frontal cortex encasing a large part of the pre-frontal cortex but not the motor cortex (pre- and post-central gyrus). The left hemisphere (fig. 11b) shows a similar pattern to the right hemisphere except for significant clusters being found at the inferior part of the pre- and post-central gyrus. Internally (fig. 11c), areas such as the Caudate nucleus, Putamen, Thalamus, and Cuneus show significant clusters.

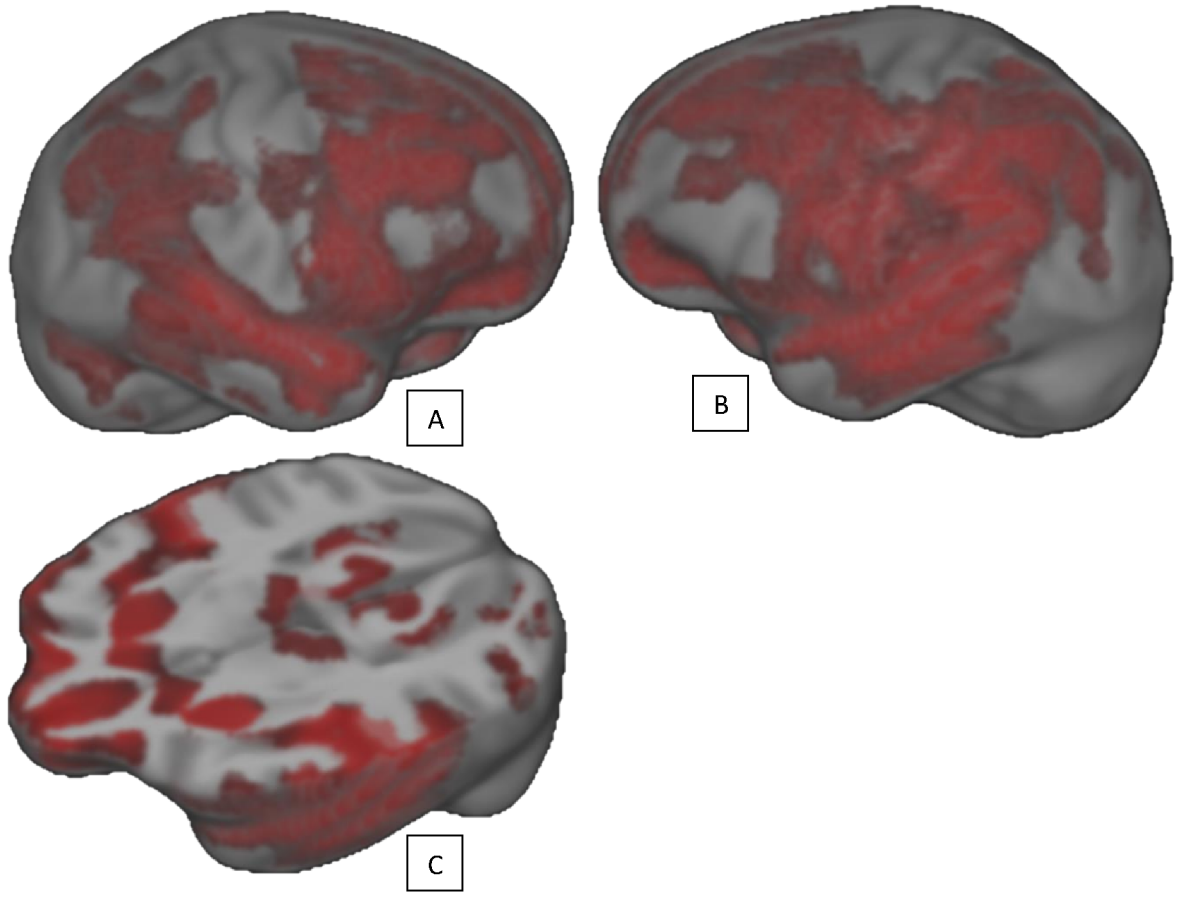

Figure 11. TFCE VBM (FWE<0.05) results from the 1.5T imaged sample of QC passed chimpanzees. Significant clusters indicate GM atrophy during aging. Clusters are presented a 3D rendering of the chimpanzee template. A shows the right lateral side of the brain, B shows the left lateral side of the brain, C shows the internal aspect of the brain.

The TFCE VBM (FWE<0.05) for the total sample of QC chimpanzees, produced multiple significant clusters across the brain (fig. 12). These clusters represent a significant GM volume loss due to aging. Figure 12a and b show similar clusters at the left and right hemisphere. There is a large significant cluster that extends the length of the temporal lobe up into the inferior parietal lobe. The frontal cortex also contains significant cluster at the posterior and middle parts of the superior, middle, and inferior frontal gyrus. There is also a large cluster at the orbito-frontal cortex. Cluster can be seen at structures within the brain (fig. 12c) such as the putamen, caudate nucleus, thalamus, and the insula.

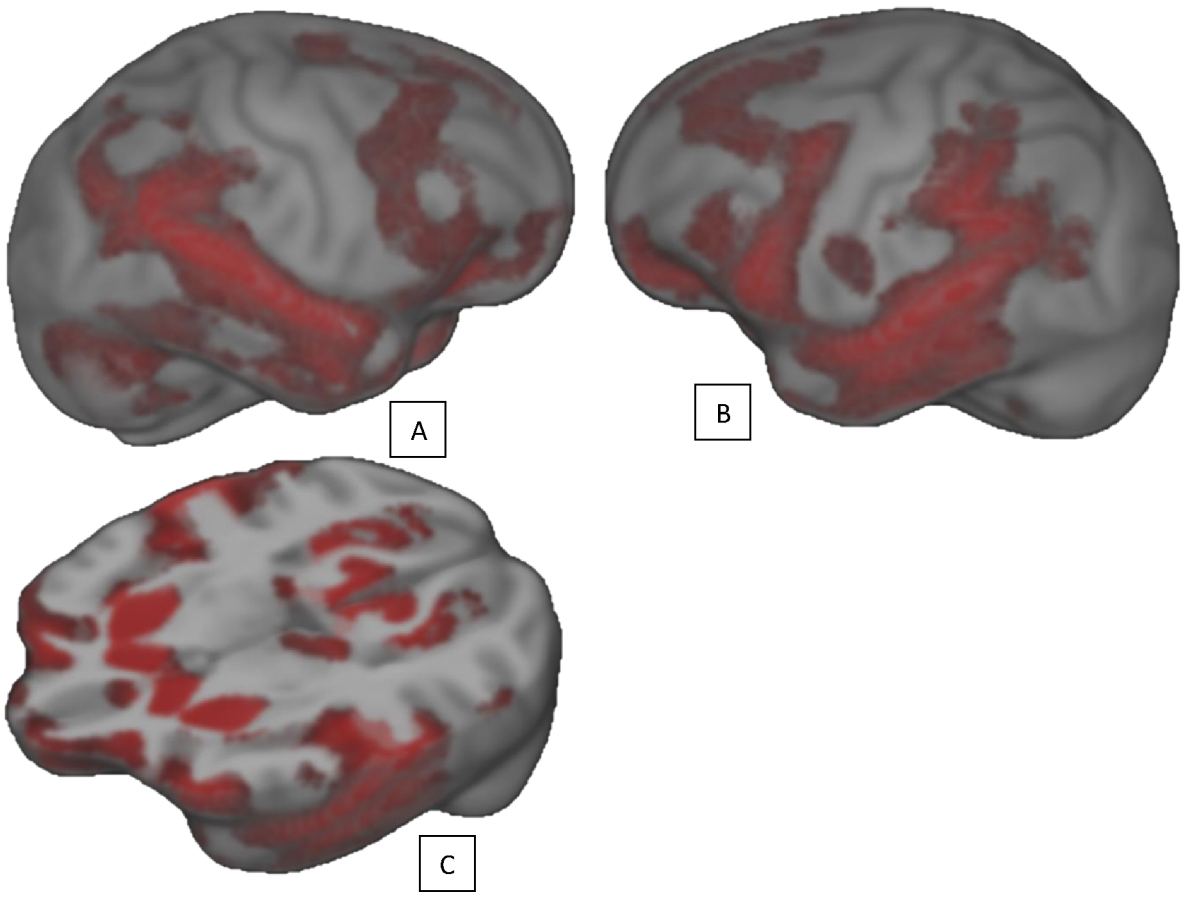

Figure 12. TFCE VBM (FWE<0.05) results from the total sample of QC passed chimpanzees. Significant clusters indicate GM atrophy during aging. Clusters are presented a 3D rendering of the chimpanzee template. A shows the right lateral side of the brain, B shows the left lateral side of the brain, C shows the internal aspect of the brain.

In summary, VBM on the 1.5T and total sample have larger and more widespread significant clusters as compared with the 3T VBM. The distribution of the significant clusters is quite similar in the 1.5T and total sample, however the clusters from the 1.5T sample spread across more of the temporal, frontal and parietal cortices.

Sex Difference VBM

Significant TFCE VBM (FWE<0.05) cluster were only found in the 3T and total sample. These clusters were in the same location for both samples, therefore one figure (fig.13) is shown. The significant clusters indicate increased GM volume in females compared to males, as there was no significant clusters found for males > females. Therefore, figure 13 illustrates

an increase in GM volume at the posterior hippocampus, parahippocampal gyrus, and at the anterior cerebellum in female compared to male chimpanzees.

Figure 13. TFCE VBM (FWE<0.05) results from the 3T imaged & total sample of QC passed chimpanzees. Significant clusters indicate increased GM volume in female compared to male chimpanzees. Clusters are presented on a 3D rendering of the chimpanzee volume template and are shown on a coronal view of the posterior part of the brain.

Non-Negative Matrix Factorization

Parcellating the chimpanzee brain into structurally co-varying regions using NNMF produced multiple components that align with known anatomical regions. The 2C, 6C, and 12C solutions for the three samples (3T, 1.5, & Total) are somewhat similar in their distribution of co-varying GM regions. Here is an outline and description of the interesting components that correspond with anatomical structures.

The 2C parcellation of the 3T sample (fig. 14a) spits the brain into one region containing the cerebellum and occipital lobe and another for the rest of the cortex. The 6C solution for the 3T sample (fig. 14b) shows the frontal cortex being roughly separated into a pre-frontal region and the pre-motor/motor area. There are also components for the occipital cortex, cerebellum, and the basal ganglia. The 12C solution (fig. 14c) follows a similar parcellation as to the 6 component solution. Where there are large co-varying region that spans the parietal and posterior temporal lobe that has 2 anterior components for the pre-frontal and motor regions, then 2 posterior components for the occipital lobe and cerebellum. With the

addition of more components in the 12C parcellation there is a further parcellation of the anterior temporal lobe, cerebellum and the medial occipital cortex.

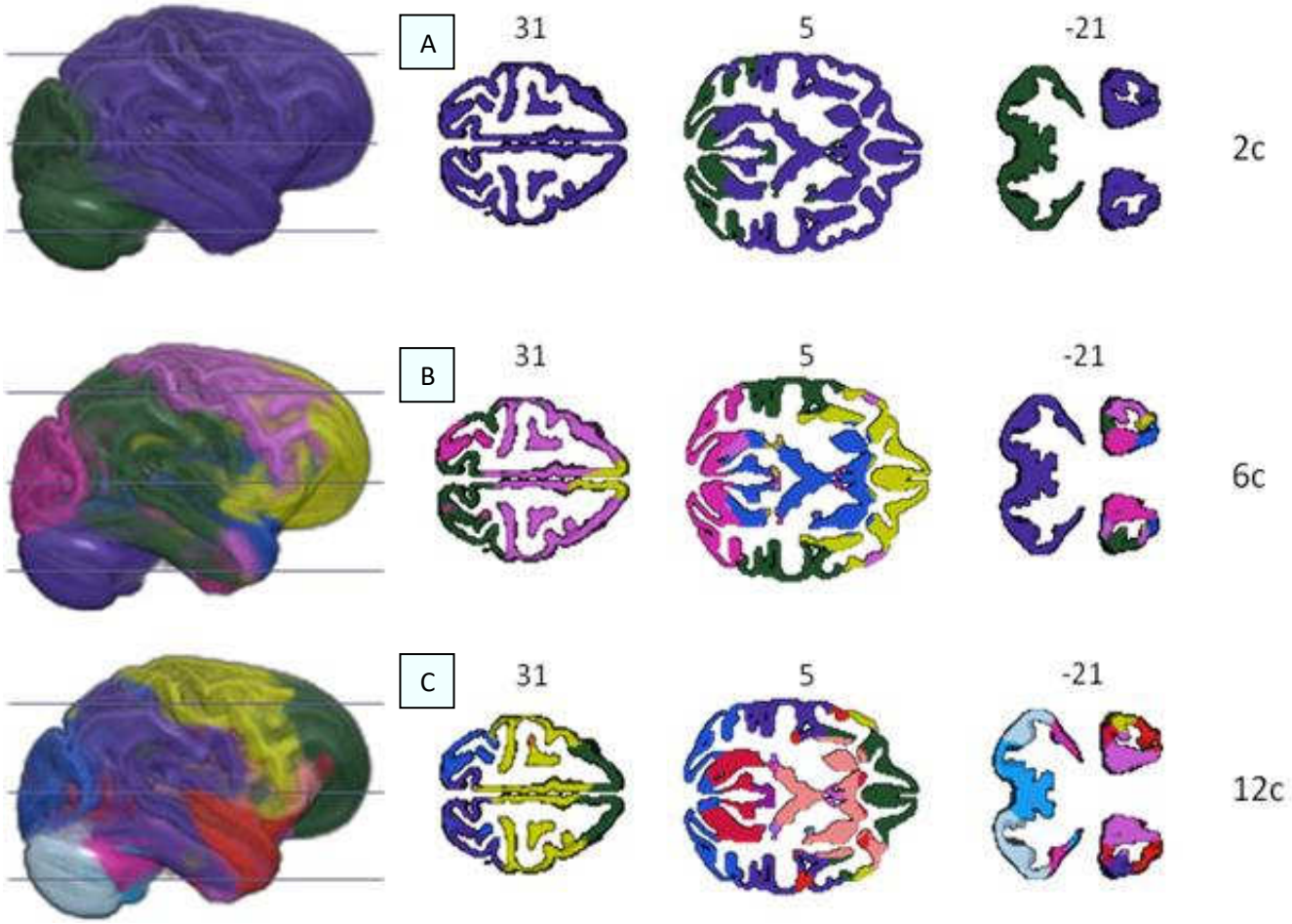

Figure 14. NNMF parcellation of the 3T chimpanzee sample. Different colors represent different NNMF components. Left is a rendering of the brain volume and right are three horizontal slices of the component solution. A, B, and C are 2, 6, and 12 component solutions respectively. Images are represented on the chimpanzee template.

The 1.5T sample NNMF 2C parcellation splits the brain into the cerebral cortex and the cerebellum (fig. 15a). Structurally co-varying regions in the 1.5T sample 6C solution (fig. 15b) align with some known brain structures, but slightly different to the 3T sample (fig. 14b). Similar to the 6C solution for the other two samples the 1.5T sample has a component that aligns with the pre-frontal cortex and the occipital cortex. Unlike the other two 6C parcellations there is a very large component that encompasses the posterior temporal lobe, inferior parietal lobe, motor cortex, and the basal ganglia.

The 12C solution of the 1.5T sample (fig. 15c) is a bit noisy has doesn't have many interesting solid components. The pre-frontal cortex component which is strongly present in the other 6C and 12C parcellations doesn't quite have the correct shape and is inter mixed with other components.

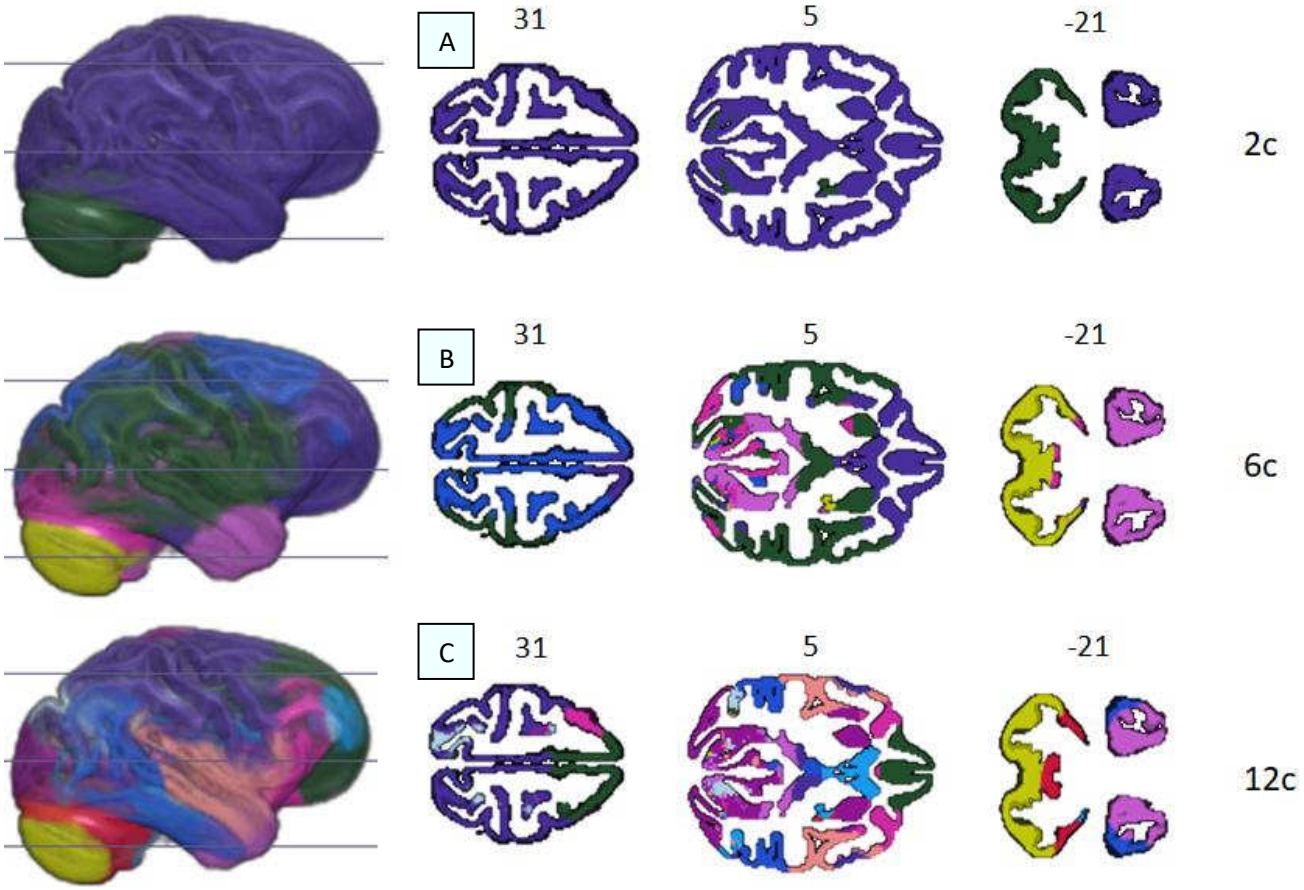

Figure 15. NNMF parcellation of the 1.5T chimpanzee sample. Different colors represent different NNMF components. Left is a rendering of the brain volume and right are three horizontal slices of the component solution. A, B, and C are 2, 6, and 12 component solutions respectively. Images are represented on the chimpanzee template.

A strange split is created by the 2C parcellation of the total sample (fig. 16a). One component is the cerebellum, occipital lobe, and part of the pre-motor cortex and pre- and post-central gyrus. The 6C solution (fig. 16b) is very similar to that of the 3T sample (fig. 14b). Where there is a component for the pre-frontal cortex, the cerebellum, and another which covers the lateral parietal cortex and most of the temporal lobe. Different to the 3T 6C parcellation is a component that encompasses the pre-motor cortex, the pre- and post-central gyrus as well as the occipital cortex.

The total samples 12 solution (fig. 16c) also produces several interesting components just like the 6 component parcellation. The pre-frontal cortex component is still present, if not a bit smaller. A component covers the whole inferior frontal gyrus as well as part of the anterior section if the temporal cortex, which has some resemblance to a component in the 12 component parcellation from the 1.5T sample. There is a component for the pre-motor and pre- and post-central gyrus which is nearly identical to one in the total 6C parcellation (fig. 16b), but this time the occipital cortex has its own component. Finally there is a component that encompasses most of the lateral parietal cortex and the posterior part of the temporal lobe as well as another component for the precuneus.

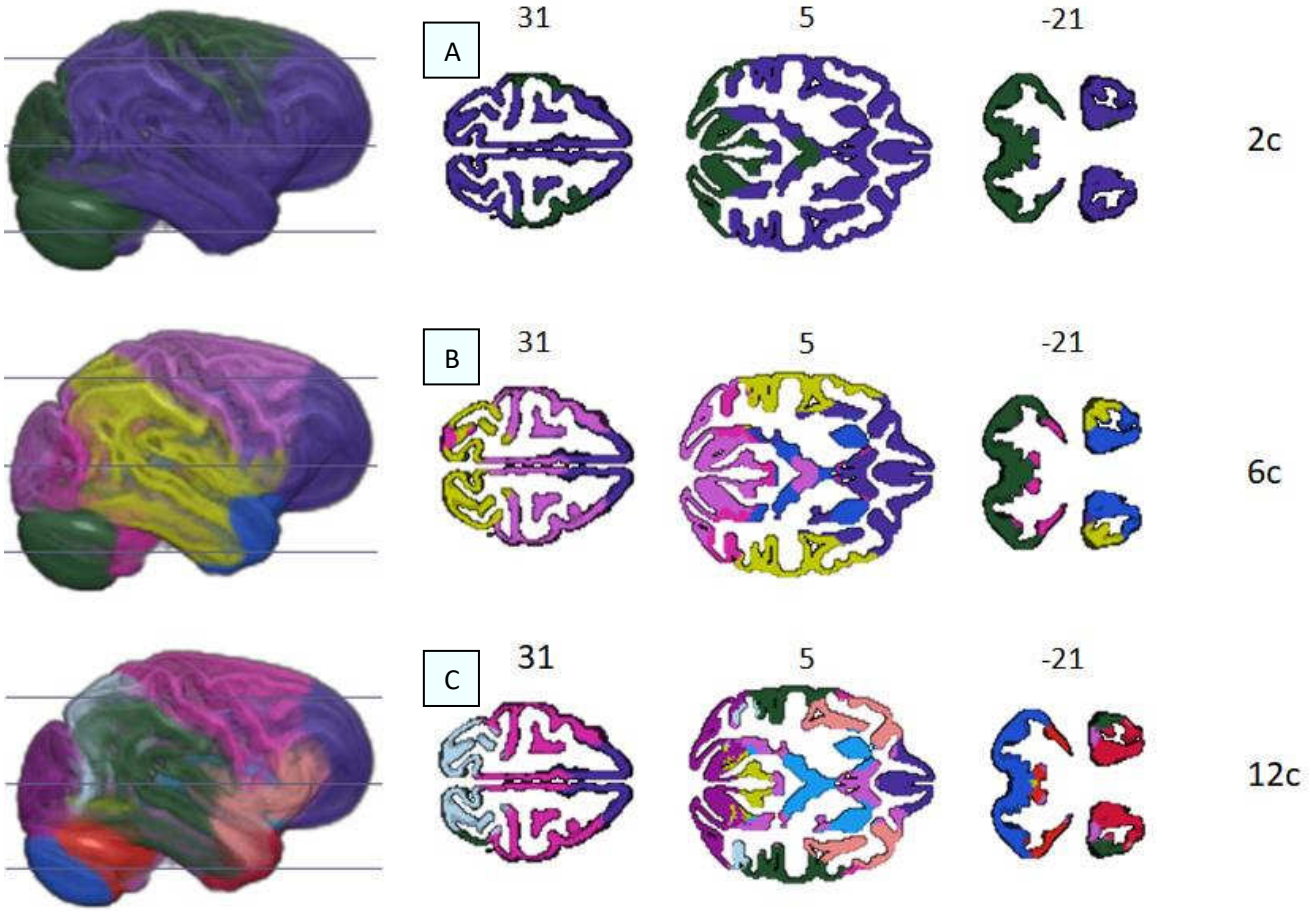

Figure 16. NNMF parcellation of the total chimpanzee sample. Different colors represent different NNMF components. Left is a rendering of the brain volume and right are three horizontal slices of the component solution. A, B, and C are 2, 6, and 12 component solutions respectively. Images are represented on the chimpanzee template.

Discussion

The present study, proposes and evaluates a chimpanzee specific structural MRI preprocessing pipeline using the CAT12 toolbox in SPM12. Evaluation was conducted in the way of GM atrophy analyzing during aging. Promising results have been presented here regarding the discovery of structural covariance GM regions within chimpanzees, by utilizing the algorithm NNMF. An aging effect on GMV decline could be successfully found using VBM, RBM, and linear regression models. The age effect shown here aligns with previously reported findings in aging chimpanzees (30, 50) and humans (51). In turn, it gives more evidence to the theory that there is an age effect on chimpanzee GM but it is not as large as in humans. The models employed all compensated for the variation in brain size, sex and scanner to ensure the effects seen were due to increased age.

Following smoothing NNMF was able to extract structurally co-varying regions that resembled some underlying cortical structures. Components were found to align with the structures prefrontal cortex, frontal/pre-motor cortex, posterior temporal/inferior parietal lobe, and the occipital cortex across the three samples 6C and 12C solutions. The results from both the age analyses and structural covariance parcellation display reasonable outcomes that can be seen as evidence for construction of an effective preprocessing pipeline.

Preprocessing Pipeline Validation

The efficacy of the chimpanzee specific preprocessing pipeline is shown by indicating GM atrophy during aging through the various methods made available from the newly created preprocessing pipeline. The age effect shown here are slightly more pronounced than those found by Chen et al. (2013) and Autrey et al. (2014) and conflicting to Sherwood et al. (2011). The sample of chimpanzees used by Sherwood et al. (2011) did not include any very old chimpanzees (> 45 years old). This may be the reason why Sherwood et al. (2011) found no age effect on total GMV, while this study and Chen et al. (2013) included multiple older chimpanzees and showed an age effect. As both of these studies contain samples with multiple very old chimpanzees. Interestingly, the study with the largest sample (30) of

chimpanzees (>200) including a relatively large amount of elderly (38 chimpanzees 40+ years old), found a significant age effect ($p = 0.033$) on GMV but this did not survive post-hoc testing.

There are several reasons for the discrepancy from the result presented in this study. Even though a relatively large sample (125) containing many elderly chimpanzees (16). A reason could be the difference in preprocessing protocols utilized. Autrey et al. (2014) preprocessed the images with BrainVISA (http://brainvisa.info) which is a software package that is optimized for sulci extraction (52). GM segment classification in this program is conducted by grey/white matter image intensity. This can lead to misclassification of tissue segments due to the partial volume effect. The partial volume effect occurs when there are two or more tissue types within a single voxel and this causes an averaging of the intensity within the voxel. Therefore, an accurate border can be difficult to define. This can become particularly difficult in lower contrast (1.5T) images, which make up a significant proportion of Autrey et al. (2014) sample (143 images). The partial volume effect can be partly compensated for by using a TPM during segmentation. Another advantage of a TPM is that one has a template for initial affine registration, which then enables the segment maps to be non-linearly registered to the corresponding segment maps of the DARTEL/Shooting templates. This means that instead of registering the entire brain to a template this is done segment to segment, for example GM to GM. Lowering the chance of registration errors that can effect results and their corresponding conclusions. Strict QC was employed in this study to ensure only the best images would be analyzed. Poor image quality can lead to misclassification of tissue segments, meaning WM can be classified as GM which can skew results. Previous aging studies in chimpanzees (30, 50, 53) did not report any QC procedures.

The unique methods used here to explain the effect aging has on GMV were RBM and VBM. These are unique as they have not been previously used in analyses of age effect on GMV in chimpanzees due, in part, to a lack of chimpanzee specific registration and segmentation templates. ROI analyses of GM decline during aging has been conducted (53) on the hippocampus and frontal cortex. Manual delineation by an expert was used and they found no significant GMV decline due to aging. This is not RBM per se, because relative volumes are not used, which can introduce errors due to intersubject brain morphology differences.

Subjectivity can also be introduced by expert drawing of the regions and as mentioned previously the sample may be too young to encompass age effects within chimpanzees. The RBM in this study indicates significant GM decline due to aging in many ROI's. A high proportion of significant results, after correcting for multiple comparisons (table 1) were found in the frontal cortex (12/15 = 80%), basal ganglia (8/12 = 67%), and the temporal lobe (17/30 = 57%). The parietal/occipital cortices (3/13 = 20%) and the motor cortex (2/15 = 13%) have a far lower proportion of significant results. The VBM results also found large significant clusters in the frontal and temporal cortices. This aligns with a study that found Alzheimer's like accumulation of amyloid beta plaques and neurofibrillary tangles in aging chimpanzees frontal and temporal brain regions (54). Aggregation of these proteins is associated with neuronal loss and cortical atrophy in humans (51, 55). Therefore, the RBM and VBM results presented here may be due to Alzheimer causing proteins, even though Alzheimer's disease is not found in chimpanzees. The amyloid plaques and neurogibillary tangles may cause neuronal loss but the noticeable cognitive decline may occur much later in the chimpanzee lifespan or be difficult to measure. The chimpanzee lifespan is 40 - 45 years in the wild and up to 60 years in captivity which may be too young to present Alzheimer's like symptoms. The aging effect on chimpanzee GMV has been shown to be quite minimal if at all (30, 50, 53). VBM is more sensitive to smaller effects as compared to an ANOVA or regression model using total GMV. The voxel-by-voxel comparison in VBM as well as compensating for intersubject morphometry differences enables this higher sensitivity. The VBM analyses on GMV sex differences in age matched groups found an increased GMV of the posterior hippocampus in females compared to males within the 3T and total sample. This is quite intriguing as there is no mention that this is the case within the chimpanzee literature, but this has been found to be the case in humans (56). Further research is therefore required to determine if this is a reproducible finding, and what could be its deeper meaning.

The aging analysis here demonstrates that the processed images can produce results that follow the same trend as stated in the literature on aging effects on the chimpanzee brain. For definitive proof of the preprocessing pipeline quantitative analysis needs to be done. One way to quantitatively prove the validity of a preprocessing pipeline is to use a phantom brain (57, 58). The phantom is a high contrast simulated brain that can be used as a gold

standard for testing accuracy and validity of registration and tissue classification algorithms. It may be difficult to find multiple very high quality images which are required for a phantom brain creation, but this would be the next step in proving the validity of the newly established pipeline.

Limitations

There are at least two potential limitations when assessing the chimpanzee specific preprocessing pipeline and the accompanying validity analysis. The preprocessing pipeline has a problem processing the 1.5T images in the sample and there are also possible cohort effects that may have influenced the validation results. The percentage of 1.5T images approx. 62%) that failed QC was significantly higher than the 3T images (approx. 8%). This may be due to the fact that a lower magnetic field produces images that are noisier and have lower contrast and quality. Therefore, the signal to noise ratio is higher in 1.5T images and may lead to poorer registration and misclassification of tissue segments. As a large proportion of the MRI data were 1.5T images, and that no new scans will be taken, the chimpanzee preprocessing pipeline needs to improve its processing of these 1.5T images. Manual segmentation by an expert can assist the algorithm to lower the chance of misclassification. This can be quite subjective and is very time consuming. Another option to deal with the problem of misclassification might be to create a separate preprocessing pipeline solely from and for the 1.5T images. This means the templates used and created will be a closer representation of the 1.5T sample, but joining these processed images with the 3T images becomes difficult especially for interpretability of results. Either way improvements need to be made so that more good quality 1.5T images can be used for analyses.

There are a number of caveats with this dataset that should be considered when assessing this study. It contains no longitudinal data, therefore the age analysis was conducted by a cross-sectional study design. Consequently, the differences exhibited in this study are between individuals of various ages and not within individual age related changes. This is particularly problematic, as aging effects on the brain is a continuous process. Therefore to capture the true age effect subjects need to be measured at two or more time points. This

study is able to partly compensate for this by having a relatively good distribution of ages within the chimpanzee cohort. Rearing experience, can have an impact on brain development and subsequent morphometry of the brain (59). A large proportion of the oldest chimpanzees in this study were wild born while most of the younger chimpanzee were born and raised in captivity. This could create a bias and hide the true aging effect, but is unavoidable as a study requires many older chimpanzees to record an age effect as shown by (30, 50). The different rearing experiences within captive chimpanzees can also have an effect on cortical organization. Chimpanzees that were reared by their mother were found to have greater white to grey matter volume and more cortical folding as compared to nursery raised chimpanzees (60). Further research is needed to understand the effect these rearing experiences have on the aging processes of the chimpanzee brain.

Two different scanners with different scanner strengths were used in this study. Unwanted variance is introduced with this. The statistical model of the whole dataset controlled for this by separating the sample into their respective scanner strengths for the various types of analyses. Figure 9 clearly shows two distinct cluster of GMV for the 3T and 1.5T samples. Whereby, the 1.5T images have a relatively lower GMV as compared to the 3T images. This is likely due to GM underestimation during preprocessing and not that the chimpanzees scanned by the 1.5T scanner had less total GMV. Nevertheless, the results shown here share resemblance with previously report results only using 3T scanned images (50). Therefore, most likely this variable did not have a great influence on the interpretability the results presented here.

Non-Negative Matrix Factorization Interpretability

The GM structural covariance parcellation obtained by NNMF not only represents statistical variation in the data, but also aligns with structural and functional networks. This is very promising as the work presented here is a proof of concept showing the applicability of this method on chimpanzees. The structural covariance analyses conducted here showed that NNMF could create a parts based representation of co-varying GM regions across individuals as well as uncover known anatomical regions. Interestingly, the 6C and 12C solutions of the three samples all have a solid component with very similar distribution that aligns with the

prefrontal cortex. The prefrontal cortex has been subject to particular neuroscientific interest as it is a hub for higher order cognitive and executive functions (61). These human-like cognitive capacities controlled by the prefrontal cortex such as complex decision making (62), imagination (63), introspection (64) and language make it particularly alluring for primate research. The ability to extract the prefrontal cortex using a data driven approach (NNMF) is shown here, which means this technique offers exciting possibilities for primate interspecies comparisons. Other structural and functional networks can be seen in the structural covariance analyses but none as apparent as the prefrontal cortex. Aside from the stable prefrontal cortex component there was a somewhat common pattern to the 6C and 12C solutions across the three samples. This was a large component for the posterior frontal/motor cortex, the posterior temporal lobe and some of the inferior parietal lobe, the occipital cortex, and finally the cerebellum. Deep insight into the structural organization of the chimpanzee brain should be cautiously taken from these relatively stable NNMF components. As there is quite some variation in these components and it is now known from the work here what is the most stable number of components for each sample. However, the ability of NNMF to extract components without any cross validation or sub-sampling that align with some anatomical structures in a moderately stable fashion, is very promising.

Symmetry is another important characteristic of the obtained parcellation. The algorithm was applied to both hemispheres simultaneously with no constraint on hemisphere symmetry. Nevertheless, the components were highly symmetrical across the two hemispheres. Giving further support to the biological interpretability of NNMF components. As the known large anatomical and functional networks are predominantly bilaterally symmetrical. Unfortunately, previously shown leftward cortical asymmetries in the chimpanzee inferior frontal gyrus and posterior temporal region (planum temporale) were unable to be shown here (65). This may be due to the low number of components used here and an increase in components might lead to uncovering these asymmetries.

This is only a pilot study to determine the effectiveness of NNMF in chimpanzee brains. Therefore, the results need to be cautiously interpreted in terms of chimpanzee brain organization. However, the possibility of NNMF being used in extracting structurally co-varying GM regions in chimpanzees is very promising. Further sub-sampling and cross

validation needs to be conducted to quantitatively determine how many components is yields the most stable component solution for each sample. The prefrontal cortex component is particularly interesting as it is shown to be quite stable here and it is very interesting for interspecies comparison due to its control over higher order cognitive functions.

Outlook

The results shown here indicate that NNMF is a viable option for extracting structurally co-varying regions of GMV in chimpanzees. Further exploration into the structural organization of the chimpanzee brain can benefit from this technique. The DaVi labeling presented here can also help in this endeavor. Comparing the similarity of the manual gyri-based parcellation with the data-driven NNMF could have a two-fold effect on understanding chimpanzee brain organization. First, a more exact and quantifiable analysis of what anatomical structures are represented by the NNMF components. This will give more biological meaning to the components. Second, the manual macroanatomical 'DaVi' labeling could benefit from reinforcement of the data driven NNMF approach. The non-subjective nature of NNMF enables more evidence for the macroanatomical labeling.

To determine the exact border between anatomical regions macroscopic parcellation is limited and one must go to the microscopic scale (16). The border of adjoining regions in the DaVi labeling is set to the middle of the corresponding sulcus. This was chosen to keep borders uniform, but a border could be at any point within the sulcus or connecting gyri. Cytoarchitectonic brain area delineation in chimpanzees (66) may be able to be spatially registered to the template created here and, in turn added to improve the DaVi labeling. This could then be applied to the large sample of chimpanzee MR images.

NNMF has be shown to work in humans and know chimpanzees a next logical step would be the comparison of the structural covariance between the two primates. Assessing the interspecies similarity of structurally co-varying regions could uncover what amount of brain organization do humans share with their closest relative, in a data driven fashion. Differences in component solutions may elude to areas that have gone through significant

evolutionary change and be human specific. In either case it offers a chance to further the understanding of primate brain development.

Comparing structurally co-varying GM regions between primates could help further understanding of the evolutionary development of primate brain organization. Understanding the similarities and differences in brain organization of macaques, chimpanzees, and humans could shed light on how the brain has changed going along the phylogenetic tree. The variation in brain structure across the three primates means a direct comparison of components is not possible. A better solution would be to compare the most stable component solutions of each primate with each other. This could help to indicate a shared organization between the species and what has changed through evolution.

Conclusion

In Conclusion, A newly established openly available chimpanzee preprocessing pipeline with accompanying chimpanzee specific TPM, DARTEL/Shooting templates, and high contrast anatomical template is explained here. The reliability of the processed images could be successfully demonstrated. This study show that chimpanzees exhibit age-related decline in both global and local GMV, which aligns with previous research on the matter (30, 50, 54). As this preprocessing pipeline has been shown to produce reliable and useable images it will be made available to the scientific community for CAT12. The DaVi labeling will also be made available as it has shown to produce predictable ROI results and can be used for automatic local GM analyses or to help with WM fiber tracking. Analyzing sex differences an unexpected but interesting difference could be seen in female chimpanzees having a increased posterior hippocampus volume as compared to males, which has been previously noticed in humans (56) but not chimpanzees. Additionally, structurally co-varying GM regions were able to be derived using NNMF that were not only statistical constructs but also aligned reasonably well with known anatomical structures. The promising results of this NNMF pilot study indicate that further study should is needed using this technique so a better understanding of the structural organization of the chimpanzee brain can be gained.

References

1. Consortium. CSA, Waterson RH, Lander ES, Wilson RK. Initial sequence of the chimpanzee genome and comparison with the human genome. Nature. 2005;437:69.
2. Rilling JK, Insel TR. The primate neocortex in comparative perspective using magnetic resonance imaging. Journal of human evolution. 1999;37(2):191-223.
3. Hopkins WD, Avants BB. Regional and hemispheric variation in cortical thickness in chimpanzees (Pan troglodytes). The Journal of neuroscience : the official journal of the Society for Neuroscience. 2013;33(12):5241-8.
4. Whiten A, Goodall J, McGrew WC, Nishida T, Reynolds V, Sugiyama Y, et al. Cultures in chimpanzees. Nature. 1999;399:682.
5. Zilles K, Armstrong E, Moser KH, Schleicher A, Stephan H. Gyrification in the cerebral cortex of primates. Brain, Behavior and Evolution. 1989;34(3):143-50.
6. Bruner E, Preuss TM, Chen X, Rilling JK. Evidence for expansion of the precuneus in human evolution. Brain structure & function. 2017;222(2):1053-60.
7. Donahue CJ, Glasser MF, Preuss TM, Rilling JK, Van Essen DC. Quantitative assessment of prefrontal cortex in humans relative to nonhuman primates. Proceedings of the National Academy of Sciences. 2018.
8. Bergfield KL, Hanson KD, Chen K, Teipel SJ, Hampel H, Rapoport SI, et al. Age-related networks of regional covariance in MRI gray matter: reproducible multivariate patterns in healthy aging. Neuroimage. 2010;49(2):1750-9.
9. Bezzola L, Merillat S, Gaser C, Jancke L. Training-induced neural plasticity in golf novices. The Journal of neuroscience : the official journal of the Society for Neuroscience. 2011;31(35):12444-8.
10. Franko E, Joly O. Evaluating Alzheimer's disease progression using rate of regional hippocampal atrophy. PloS one. 2013;8(8):e71354.
11. Ashburner J, Neelin P, Collins DL, Evans A, Friston K. Incorporating prior knowledge into image registration. Neuroimage. 1997;6(4):344-52.
12. Ashburner J, Friston KJ. Nonlinear spatial normalization using basis functions. Human brain mapping. 1999;7(4):254-66.
13. Ashburner J, Friston KJ. Voxel-based morphometry--the methods. Neuroimage. 2000;11(6 Pt 1):805-21.
14. Ashburner J, Friston KJ. Unified segmentation. Neuroimage. 2005;26(3):839-51.
15. Mechelli A, Price CJ, Friston KJ, Ashburner J. Voxel-based morphometry of the human brain: Methods and applications. CURRENT MEDICAL IMAGING REVIEWS. 2005;1(2):105-13.
16. Eickhoff SB, Stephan KE, Mohlberg H, Grefkes C, Fink GR, Amunts K, et al. A new SPM toolbox for combining probabilistic cytoarchitectonic maps and functional imaging data. Neuroimage. 2005;25(4):1325-35.
17. Palomero-Gallagher N, Zilles K. Cyto- and receptor architectonic mapping of the human brain. Handbook of clinical neurology. 2018;150:355-87.
18. Alexander-Bloch A, Giedd JN, Bullmore E. Imaging structural co-variance between human brain regions. Nature reviews Neuroscience. 2013;14(5):322-36.
19. Mechelli A, Friston KJ, Frackowiak RS, Price CJ. Structural covariance in the human cortex. The Journal of neuroscience : the official journal of the Society for Neuroscience. 2005;25(36):8303-10.
20. Andrews TJ, Halpern SD, Purves D. Correlated size variations in human visual cortex, lateral geniculate nucleus, and optic tract. The Journal of neuroscience : the official journal of the Society for Neuroscience. 1997;17(8):2859-68.
21. Lerch JP, Worsley K, Shaw WP, Greenstein DK, Lenroot RK, Giedd J, et al. Mapping anatomical correlations across cerebral cortex (MACACC) using cortical thickness from MRI. Neuroimage. 2006;31(3):993-1003.

22. Bohbot VD, Lerch J, Thorndycraft B, Iaria G, Zijdenbos AP. Gray matter differences correlate with spontaneous strategies in a human virtual navigation task. The Journal of neuroscience : the official journal of the Society for Neuroscience. 2007;27(38):10078-83.
23. Alexander-Bloch A, Raznahan A, Bullmore E, Giedd J. The convergence of maturational change and structural covariance in human cortical networks. The Journal of neuroscience : the official journal of the Society for Neuroscience. 2013;33(7):2889-99.
24. Alexander GE, Chen K, Aschenbrenner M, Merkley TL, Santerre-Lemmon LE, Shamy JL, et al. Age-related regional network of magnetic resonance imaging gray matter in the rhesus macaque. The Journal of neuroscience : the official journal of the Society for Neuroscience. 2008;28(11):2710-8.
25. Pagani M, Bifone A, Gozzi A. Structural covariance networks in the mouse brain. Neuroimage. 2016;129:55-63.
26. Sotiras A, Resnick SM, Davatzikos C. Finding imaging patterns of structural covariance via Non-Negative Matrix Factorization. Neuroimage. 2015;108:1-16.
27. Lee DD, Seung HS. Learning the parts of objects by non-negative matrix factorization. Nature. 1999;401(6755):788-91.
28. Sotiras A, Toledo JB, Gur RE, Gur RC, Satterthwaite TD, Davatzikos C. Patterns of coordinated cortical remodeling during adolescence and their associations with functional specialization and evolutionary expansion. Proceedings of the National Academy of Sciences of the United States of America. 2017;114(13):3527-32.
29. Varikuti DP, Genon S, Sotiras A, Schwender H, Hoffstaedter F, Patil KR, et al. Evaluation of non-negative matrix factorization of grey matter in age prediction. Neuroimage. 2018;173:394-410.
30. Autrey MM, Reamer LA, Mareno MC, Sherwood CC, Herndon JG, Preuss T, et al. Age-related effects in the neocortical organization of chimpanzees: gray and white matter volume, cortical thickness, and gyrification. Neuroimage. 2014;101:59-67.
31. Manjon JV, Coupe P, Marti-Bonmati L, Collins DL, Robles M. Adaptive non-local means denoising of MR images with spatially varying noise levels. Journal of magnetic resonance imaging : JMRI. 2010;31(1):192-203.
32. Ashburner J. Computational anatomy with the SPM software. Magnetic resonance imaging. 2009;27(8):1163-74.
33. Dahnke R, Ziegler G, Gaser C. Local Adaptive Segmentation. Human Brain Mapping Conference; Beijing2012.
34. Dahnke R, Yotter RA, Gaser C. Partitioning of the brain using graph-cut. Human brain mapping; Barcelona2010.
35. Rajapakse JC, Giedd JN, Rapoport JL. Statistical approach to segmentation of single-channel cerebral MR images. IEEE transactions on medical imaging. 1997;16(2):176-86.
36. Dahnke R, Gaser C. Voxel-based Preprocessing in CAT. Organisation of Human Brain Mapping; Vancouver2017.
37. Ashburner J. A fast diffeomorphic image registration algorithm. Neuroimage. 2007;38(1):95-113.
38. Ashburner J, Friston KJ. Diffeomorphic registration using geodesic shooting and Gauss–Newton optimisation. Neuroimage. 2011;55(3-3):954-67.
39. Beg MF, Miller M, Trouvé A, Younes L. Computing Large Deformation Metric Mappings via Geodesic Flows of Diffeomorphisms2005. 139-57 p.
40. Franke K, Clarke GD, Dahnke R, Gaser C, Kuo AH, Li C, et al. Premature Brain Aging in Baboons Resulting from Moderate Fetal Undernutrition. Frontiers in Aging Neuroscience. 2017;9:92.
41. Desikan RS, Segonne F, Fischl B, Quinn BT, Dickerson BC, Blacker D, et al. An automated labeling system for subdividing the human cerebral cortex on MRI scans into gyral based regions of interest. Neuroimage. 2006;31(3):968-80.

42. Hopkins WD, Li X, Crow T, Roberts N. Vertex- and atlas-based comparisons in measures of cortical thickness, gyrification and white matter volume between humans and chimpanzees. Brain structure & function. 2017;222(1):229-45.
43. Zilles K, Rehkaemper G. Funktionelle Neuroanatomie Berlin ;Heidelberg ;New York: Springer; 1998.
44. Mai JK, Majtanik M, Paxinos G. Atlas of the Human Brain: Elsevier Science; 2015.
45. Diedrichsen J. A spatially unbiased atlas template of the human cerebellum. Neuroimage. 2006;33(1):127-38.
46. Reuter M, Tisdall MD, Qureshi A, Buckner RL, van der Kouwe AJW, Fischl B. Head motion during MRI acquisition reduces gray matter volume and thickness estimates. Neuroimage. 2015;107:107-15.
47. Benjamini Y, Hochberg Y. Controlling The False Discovery Rate - A Practical And Powerful Approach To Multiple Testing1995. 289-300 p.
48. Boutsidis C, Gallopoulos E. SVD based initialization: A head start for nonnegative matrix factorization. Pattern Recogn. 2008;41(4):1350-62.
49. Yang Z, Oja E. Linear and nonlinear projective nonnegative matrix factorization. IEEE transactions on neural networks. 2010;21(5):734-49.
50. Chen X, Errangi B, Li L, Glasser MF, Westlye LT, Fjell AM, et al. Brain aging in humans, chimpanzees (Pan troglodytes), and rhesus macaques (Macaca mulatta): magnetic resonance imaging studies of macro- and microstructural changes. Neurobiology of aging. 2013;34(10):2248-60.
51. La Joie R, Perrotin A, Barre L, Hommet C, Mezenge F, Ibazizene M, et al. Region-specific hierarchy between atrophy, hypometabolism, and beta-amyloid (Abeta) load in Alzheimer's disease dementia. The Journal of neuroscience : the official journal of the Society for Neuroscience. 2012;32(46):16265-73.
52. Mangin JF, Riviere D, Cachia A, Duchesnay E, Cointepas Y, Papadopoulos-Orfanos D, et al. Object-based morphometry of the cerebral cortex. IEEE transactions on medical imaging. 2004;23(8):968-82.
53. Sherwood CC, Gordon AD, Allen JS, Phillips KA, Erwin JM, Hof PR, et al. Aging of the cerebral cortex differs between humans and chimpanzees. Proceedings of the National Academy of Sciences of the United States of America. 2011;108(32):13029-34.
54. Edler MK, Sherwood CC, Meindl RS, Hopkins WD, Ely JJ, Erwin JM, et al. Aged chimpanzees exhibit pathologic hallmarks of Alzheimer's disease. Neurobiology of aging. 2017;59:107-20.
55. Llado A, Tort-Merino A, Sanchez-Valle R, Falgas N, Balasa M, Bosch B, et al. The hippocampal longitudinal axis-relevance for underlying tau and TDP-43 pathology. Neurobiology of aging. 2018;70:1-9.
56. Persson J, Spreng RN, Turner G, Herlitz A, Morell A, Stening E, et al. Sex differences in volume and structural covariance of the anterior and posterior hippocampus. Neuroimage. 2014;99:215-25.
57. Aubert-Broche B, Evans AC, Collins L. A new improved version of the realistic digital brain phantom. Neuroimage. 2006;32(1):138-45.
58. Collins DL, Zijdenbos AP, Kollokian V, Sled JG, Kabani NJ, Holmes CJ, et al. Design and construction of a realistic digital brain phantom. IEEE transactions on medical imaging. 1998;17(3):463-8.
59. Schenker NM, Desgouttes AM, Semendeferi K. Neural connectivity and cortical substrates of cognition in hominoids. Journal of human evolution. 2005;49(5):547-69.
60. Bogart SL, Bennett AJ, Schapiro SJ, Reamer LA, Hopkins WD. Different early rearing experiences have long term effects on cortical organization in captive chimpanzees (Pan troglodytes). Developmental science. 2014;17(2):161-74.
61. Wood JN, Grafman J. Human prefrontal cortex: processing and representational perspectives. Nature reviews Neuroscience. 2003;4(2):139-47.

62. Miller EK, Cohen JD. An integrative theory of prefrontal cortex function. Annual review of neuroscience. 2001;24:167-202.
63. Schacter DL, Addis DR, Buckner RL. Remembering the past to imagine the future: the prospective brain. Nature reviews Neuroscience. 2007;8(9):657-61.
64. Fleming SM, Weil RS, Nagy Z, Dolan RJ, Rees G. Relating introspective accuracy to individual differences in brain structure. Science (New York, NY). 2010;329(5998):1541-3.
65. Hopkins WD, Adams MJ, Weiss A. Genetic and Environmental Contributions to the Expression of Handedness in Chimpanzees (Pan troglodytes). Genes, brain, and behavior. 2013;12(4):446-52.
66. Schenker NM, Buxhoeveden DP, Blackmon WL, Amunts K, Zilles K, Semendeferi K. A comparative quantitative analysis of cytoarchitecture and minicolumnar organization in Broca's area in humans and great apes. The Journal of comparative neurology. 2008;510(1):117-28.